Surv Geophys (2017) 38:1043–1096
https://doi.org/10.1007/s10712-017-9424-4

A Review of Recent Developments in the Study of Regional Lithospheric Electrical Structure of the Asian Continent

Letian Zhang[1,2]

Received: 7 December 2016 / Accepted: 3 September 2017 / Published online: 15 September 2017

Abstract The Asian continent was formed through the amalgamation of several major continental blocks that were formerly separated by the Paleo-Asian and Tethyan Oceans. During this process, the Asian continent underwent a long period of continental crustal growth and tectonic deformation, making it the largest and youngest continent on Earth. This paper presents a review of the application of geophysical electromagnetic methods, mainly the magnetotelluric (MT) method, in recent investigations of the diverse tectonic features across the Asian continent. The case studies cover the major continental blocks of Asia, the Central Asian orogenic system, the Tethyan orogenic system, as well as the western Pacific subduction system. In summary, most of the major continental blocks of Asia exhibit a three-layer structure with a resistive upper crust and upper mantle and a relatively conductive mid-lower crust. Large-scale conductors in the upper mantle were interpreted as an indication of lithospheric modification at the craton margins. The electrical structure of the Central Asian orogenic system is generally more resistive than the bordering continental blocks, whereas the Tethyan orogenic system displays more conductive, with pervasive conductors in the lower crust and upper mantle. The western Pacific subduction system shows increasing complexity in its electrical structure from its northern extent to its southern extent. In general, the following areas of the Asian continent have increasingly conductive lithospheric electrical structures, which correspond to a transition from the most stable areas to the most active tectonic areas of Asia: the major continental blocks, the accretionary Central Asian orogenic system, the collisional Tethyan orogenic system, and the western Pacific subduction system. As a key part of this review, a three-dimensional (3-D) model of the lithospheric electrical structure of a large portion of the Tibetan Plateau is presented and discussed in detail; the model indicates tearing of the

✉ Letian Zhang
letianOI@gmail.com

[1] Key Laboratory of Geo-detection (China University of Geosciences, Beijing), Ministry of Education, Beijing 100083, China

[2] School of Geophysics and Information Technology, China University of Geosciences, Beijing 100083, China

underthrusting Indian slab as well as complex crustal conductor geometries, which are not obviously consistent with the hypothesis of a continuous, eastward channel flow. These studies have greatly enhanced our knowledge of the formation and deformation processes of the Asian continent. Lastly, future research to expand field data coverage, improve related techniques, and integrate data from other disciplines is suggested.

Keywords Lithospheric electrical structure · Asia · Continental blocks · Orogenic and subduction systems · Tibetan Plateau

1 Introduction

Asia is the largest continent on Earth. This continent covers an area of approximately 44 million km^2, which is approximately 30% of the total continental area and 8.7% of the total surface area of Earth. The Asian continent is bounded by the Arctic Ocean to the north, the Pacific Ocean to the east, and the Indian Ocean to the south. The Eurasian Plate includes most of Asia and Europe, and there is no clear physical boundary between the Asian continent and the European continent to the west. However, it is generally considered that the two continents are separated along the lineament formed by, from north to south, the Ural Mountains, the Ural River, the Caucasus Mountains, and the southern margin of the Black Sea.

In addition to its vast area, formed through the amalgamation of several major continental blocks, such as the Siberia, Tarim, North China, South China, Arabia, India, and Indochina blocks, Asia is also the youngest continent of Earth (Safonova and Maruyama 2014; Yin 2010). It should be noted that the region of Kazakhstan was once considered as one of the cratonic nuclei that formed the Asian continent. However, recent structural geology and geochronology studies have suggested that the "Kazakhstan block" is a collage system and forms an orocline that is part of the Central Asian Orogenic Belt (Xiao et al. 2015b). These nuclei had been separated by the Paleo-Asian and Tethyan Oceans and their branches and finally aggregated into the tectonic framework that created the Asian continent during the Phanerozoic, when the Paleo-Asian and Tethyan Oceans closed (see Fig. 1). During this process, the Asian continent underwent a long period of continental crustal growth and tectonic deformation, leading to the formation of two of the largest orogenic systems, namely the Central Asian orogenic system and the Tethyan orogenic system. In the Tethyan orogenic system, the ongoing indentation of the Arabian and Indian Plates still plays a significant role in controlling the large-scale, active tectonics in Asia. On the eastern margin of the Asian continent, the western Pacific subduction system forms the western part of the Pacific "Ring of Fire," along which strong earthquakes and volcanic activity occur. Therefore, Asia is the continent with the most diverse and complex patterns of active deformation (Yin 2010).

To understand the complex evolution and deformation mechanisms of the Asian continent, geophysical electromagnetic (EM) methods, primarily the magnetotelluric (MT) method, have been extensively used during the past decades to image the subsurface electrical structure. The MT method is a frequency-domain electromagnetic method that detects the distribution of electrical resistivity (or its reciprocal, electrical conductivity) from near-surface depths to the lithosphere–asthenosphere boundary (LAB) by inverting the frequency-dependent impedance tensor and/or the vertical magnetic transfer function (VTF) data that are derived from recording the natural electrical and magnetic fields at the surface of the Earth. A systematic introduction of the technical details of the MT method

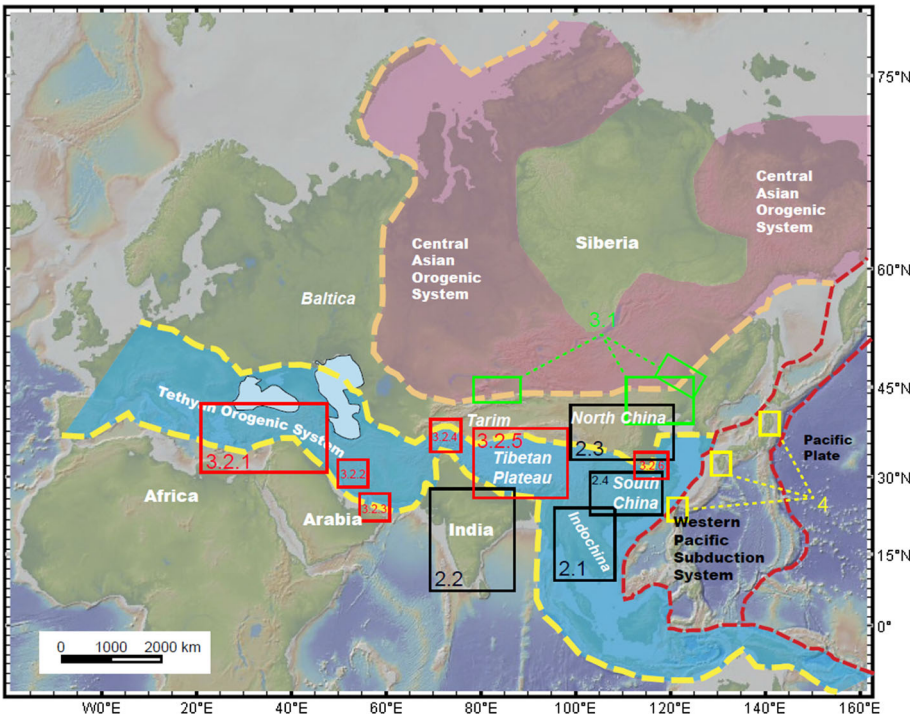

Fig. 1 Simplified tectonic map of the Asian continent (modified after Wu et al. 2016). Rectangles of different colors indicate regions discussed in the following sections of this review

can be found in a book by Chave and Jones (2012). In addition to the MT method, EM methods based on long-term monitoring, such as the magnetovariation (GMV) and geomagnetic deep sounding (GDS) methods, are also occasionally used to image the subsurface electrical structure to the depth of the mantle transition zone (MTZ). These methods image the subsurface electrical resistivity, which is a rock property that is sensitive to the presence of fluids and temperature, and can provide important constraints on the lithospheric rheology (Liu and Hasterok 2016).

In this review, case studies are presented to highlight the recent developments in the study of the regional lithospheric electrical structure of the Asian continent. Following a similar classification of case studies in a previous review by Jones (1992) on the electrical conductivity of the continental lower crust, these studies are arranged according to the various tectonic features that they are focused on. I will begin with case studies from the major continental blocks, including regions of the Indochina, India, North China and South China blocks (black rectangles in Fig. 1). These case studies will be followed by case studies of the two major orogenic systems of Asia, namely the Central Asian orogenic system (green rectangles in Fig. 1) and the Tethyan orogenic system (red rectangles in Fig. 1), with emphasis on the latter. Both orogenic systems will be discussed from their western to eastern extents. Regarding the Tethyan orogenic system, I will discuss case studies covering the regions of, from its western to eastern extents, the North and East Anatolian faults, the Zagros collision belt, the Oman ophiolite suite, Pamir, and the Tibetan Plateau and its surrounding regions, as well as the Qinling-Dabie Orogen. As a key part of

this review, a three-dimensional (3-D) model of the lithospheric electrical structure of a large portion of the Tibetan Plateau will be presented and discussed in detail. The final part of this review will be focused on the western Pacific subduction system. Three MT studies of the northeast Japan subduction zone, Kyushu subduction zone, and Taiwan orogen (yellow rectangles in Fig. 1) along this subduction system will be introduced from north to south and discussed. A detailed summary of all the case studies discussed in this review is provided in Table 1, which includes a comparison of the common and distinct features between these case studies. More detailed discussion is provided at the end of each section as well as in the conclusions. Suggestions for future studies are also provided at the end of this review.

2 Lithospheric Electrical Structure of the Major Continental Blocks

2.1 Indochina

The Indochina peninsula is located south of the South China block and east of the Indian Plate (see Fig. 2). The Indochina peninsula forms the continental portion of Southeast Asia. This region is bounded by the Red River Fault to the east and the Sagaing Fault to the west. Both faults are large-scale strike-slip faults, and the region displays the typical pattern of extrusion tectonics. The southeastward extrusion of Indochina may be associated with the convergence between the Indian Plate and the Eurasian Plate (Yin 2010). The Indochina peninsula could be further divided into four micro-blocks, namely, from west to the east, the West Burma Block, the Shan-Thai Block, the Lampang-Chiang Rai block, and the Indochina Block (Fig. 2). In the Triassic, the westward subduction of the Lampang-Chiang Rai block beneath the Shan-Thai Block marks the closure of the Paleo-Tethys Ocean. The eastward subduction of the West Burma Block beneath the Shan-Thai Block closed the Meso-Tethys Ocean during the early Tertiary.

A 3-D MT array has been deployed in the central Shan-Thai Block (Kanchanaburi Province, western Thailand) to investigate the subsurface electrical structure associated with the aforementioned subduction (Boonchaisuk et al. 2013). MT data from 39 stations across the study area were collected and inverted with the parallel version of the WSINV3DMT-VTF code (Siripunvaraporn and Egbert 2009; Siripunvaraporn et al. 2005) to construct a 3-D electrical structure model of the study region (see Fig. 3a, b). From the inversion model, the mid and lower crusts are conductive. Based on the average resistivity of less than 100 Ωm and the Hashin–Shtrikman upper-bound approximation, this conductive area is interpreted as mafic granulites with 3% porosity, in which the remnant dehydrated fluid accumulated during the subduction process. Two large-scale conductors are observed in the western and eastern parts of the study area (marked as WC and EC in Fig. 3b). These two conductors are interpreted as mafic and ultramafic intrusions produced by the eastward and westward subduction zones, respectively. The observations of the two large-scale conductors and the conductive lower crust support the hypothesis of a dual subduction zone in this area during the middle Triassic to Miocene, as shown in Fig. 3c.

2.2 India

The Indian subcontinent forms the southern region of Asia. This subcontinent consists of various cratonic blocks with differing ages, namely the Dharwar, Bastar, Singhbhum,

Table 1 List of case studies discussed in this review with method specifics, typical resistivity values, as well as major tectonic features

Location	References	Method specifics	Typical resistivity (Ωm)			Major tectonic features
			Upper crust	Mid-lower crust	Upper mantle	
Major Continent blocks						
Indochina						
Central Shan-Thai Block	Boonchaisuk et al. (2013)	MT array, 39 stations, 3D data-space OCCAM inversion (WSINV3DMT)	>10,000	~100	—	Two conductors <10 Ωm represent mafic/ultramafic intrusions produced by ancient subduction, support hypotheses of dual subduction zones.
India						
Dharwar craton	Gokarn et al. (2004)	MT profile, 43 stations, 2D NLCG inversion	>5000	~500	~10000	LAB depth 80–100 km, deepen eastward beneath EDC with a maximum depth of ~160 km.
	Naganjaneyulu and Santosh (2012)	MT profile, 5 stations, 2D NLCG inversion	>10,000	~500	~5000	Lower limit of 175 km for the LAB depth of EDC.
	Abdul Azeez et al. (2015)	MT profile, 44 stations, 2D NLCG inversion	~10,000	~100	~5000	Large-scale conductor (20–100 Ωm) between Coorg block and WDC, as well as in the upper mantle beneath western WDC, indicates modification of Dharwar lithosphere. Thick lithosphere (~190 km) is preserved beneath eastern WDC.
Southern granulite terrain	Patro et al. (2014)	2 MT profiles, 50 stations, 3D data-space OCCAM inversion (WSINV3DMT)	>5000	~500	~1000	Northern segment: thick resistive upper mantle; southern segment: relatively thinned lithosphere.

Table 1 continued

Location	References	Method specifics	Typical resistivity (Ωm)			Major tectonic features
			Upper crust	Mid-lower crust	Upper mantle	
Deccan volcanic province	Patro and Sarma (2009)	3 MT profiles, 57 stations, 2D NLCG inversion	>5000	~500	Top: ~5000 Bottom: ~100	Two layered lithospheric mantle structures with a resistive top layer and a conductive bottom layer in 50–200 km depth; mantle conductor beneath DVP in the depth range of 80–120 km.
Central Indian Tectonic Zone	Abdul Azeez et al. (2013)	5 MT profiles, 97 stations, 2D NLCG inversion	>3000	10-80	~5000	Widespread conductive zones in mid-lower crust are associated with fluids, which explain the persistent weakness of CITZ; North-dipping conductive layer supports northward polarity of the subduction process that formed the CITZ.
North China						
Ordos Block	Dong et al. (2014)	MT array, 150 stations, 3D data-space OCCAM inversion (WSINV3DMT)	300–1000	North: ~10 South: 100–300	North: ~10 South: 300–1000	Prominent lithospheric conductor extends from upper mantle to mid-lower crust beneath northern Ordos, indicating regional modification and lithospheric thinning.
North China	Xu et al. (2015)	14 GDS stations, 1D Occam inversion	—	—	West: 10–100 East: 2–30	MTZ conductivity beneath Eastern Block is 2 ~ 5 times higher than the Ordos Block, which might be associated with subduction process of the Pacific Plate.

Table 1 continued

Location	References	Method specifics	Typical resistivity (Ωm)			Major tectonic features
			Upper crust	Mid-lower crust	Upper mantle	
South China	Zhang et al. (2015a)	MT profile, 99 stations, 2D NLCG inversion	Yangtze: 10–100 Others: >1000	Eastern Yangtze: ~10 Others: ~1000	Eastern Yangtze: ~10–100 Others: ~1000	Resistive bulks of western Yangtze block, Jiangnan orogen, and Cathaysia block separated by conductive eastern Yangtze block and Jiangshao fault; Intra-continental Jiangnan orogen is formed along paleo-suture, where the lithosphere is relatively weak and easy to be deformed.
Central Asian orogenic system						
Western Junggar	Xu et al (2016a)	MT profile, 60 stations, 3D NLCG inversion (ModEM)	~1000	~100	<100	MT transect suggests a fossil intra-oceanic subduction system with the polarity from SE to NW beneath the western Junggar accretionary collage and western Junggar basin.
NE margin of North China Craton	Dong et al. (2015)	MT profile, 48 stations, 2D NLCG inversion	~1000	~100	CAOB: 300–1000 NE NCC: <100	NW-dipping crustal conductor beneath the Solonker suture; CAOB: relatively thick lithosphere with resistive upper mantle; NE NCC thin lithosphere with conductive upper mantle.
Great Xing'an range	Liang et al. (2015)	MT profile, 98 stations, 2D NLCG inversion	>1500	<100	~1000	Upper crust is mainly composed of resistive volcanic rocks; large-scale resistor in the lithospheric mantle implies lower crust delamination; lithospheric west-dipping conductor is inferred as residual convergence zone between GXR and Songliao Basin.

Table 1 continued

Location	References	Method specifics	Typical resistivity (Ωm)			Major tectonic features
			Upper crust	Mid-lower crust	Upper mantle	
Tethyan orogenic system						
North and East Anatolian Faults	Kaya et al. (2013)	4 MT profiles, 58 stations, Modified 2D OCCAM inversion incorporating static shift parameters	~1000	~10	~10	Subvertical conductor extends from ~10 km into upper mantle beneath western end of NAF; Continuous electrical structure beneath NAF from onland areas into the Marmara Sea.
	Türkoğlu et al (2008, 2015)	5 MT profiles, 131 stations, 2D NLCG inversion	~1000	~10	10–300	Eastern Anatolian Block is characterized by pervasive lower crust conductors underlain by relatively normal upper mantle; Both NAF and EAF are underlain by a subvertical conductor extending into the lower crust.
Zagros Collision Belt	Oskooi et al. (2014)	MT profile, 46 stations, 2D data-space OCCAM inversion	Arabia: ~10 Eurasia: ~100	Arabia: 10–100 Eurasia: ~1000	Arabia: ~100 Eurasia: ~1000	Transition between Arabia and Eurasia consists of a series of conductors and resistors with complex geometry; Arabian Plate is more conductive than Eurasian Plate down to the depth of 100 km.
	Oskooi et al. (2015)	MT profile, 18 stations, 2D data-space OCCAM inversion	>1000	—	—	Neyriz Ophiolite assemblage performs highly resistive, while the Sanandaj–Sirjan metamorphic zone and Main Zagros Thrust are more conductive.

Table 1 continued

Location	References	Method specifics	Typical resistivity (Ωm)			Major tectonic features
			Upper crust	Mid-lower crust	Upper mantle	
Oman Ophiolite Suite	Thiel et al. (2009)	MT profile, 16 stations, 2D NLCG inversion	1000–10000	100–1000	~1000	Most resistivity interfaces dip southwestward, suggesting early-stage subduction of the oceanic lithosphere beneath the Arabian continental margin prior to the ophiolite emplacement.
Pamir	Sass et al. (2014)	MT profile, 177 stations, 2D NLCG inversion, 3D NLCG inversion (ModEM)	~1000	1–10	—	Upper crust of paleo-suture zones are conductive, whereas metamorphic rocks in Central Pamir are highly resistive; Laterally extended conductive zone indicates mid-lower crustal flow underneath Southern Pamir; Mid-lower crust conductors of Central and Northern Pamir likely record fluids released by metamorphism associated with active continental subduction/ delamination.

Table 1 continued

Location	References	Method specifics	Typical resistivity (Ωm)			Major tectonic features
			Upper crust	Mid-lower crust	Upper mantle	
Tibetan Plateau	This study	MT array, 102 stations, 3D NLCG inversion (ModEM)	~1000	1–10	India: ~1000 Eurasia 1–30	Complex distribution of widespread crustal conductors is not consistent with the continuous eastward channel flow model, but rather suggests N–S extension; Southern Qiangtang and central Lhasa Terranes are identified as the two most conductive regions in the upper mantle; Underthrust Indian plate can be traced beneath the Bangong–Nujiang suture in western Tibet, but only beneath the central Lhasa terrane in central Tibet, which might be associated with tearing of the underthrusting Indian slab.
Dabie Orogen	Xu et al. (2016b)	MT profile, 56 stations, 3D NLCG inversion (ModEM)	>10,000	~10	West: ~1000 East ~100	Eastern Dabie: refertilized lithospheric mantle with elevated electrical conductivity; lowermost crust was removed by delamination during the orogenic collapse; Western Dabie: residual cratonic crust is underlain by depleted lithospheric mantle with relatively high resistivity.

Table 1 continued

Location	References	Method specifics	Typical resistivity (Ωm)			Major tectonic features
			Upper crust	Mid-lower crust	Upper mantle	
Western Pacific subduction system						
NE Japan Subduction Zone	Ichiki et al. (2015)	MT array, 59 stations, 3D data-space OCCAM inversion (WSINV3DMT) with prior information of subducting slab	<10	~1000	PCP: ~5000 EUP: ~100	Vertically continuous conductor <10 Ωm is imaged from the subducting slab surface to the lower crust, indicating a saline fluid and/or melt pathway; Shape of conductor indicates the presence of small-scale poloidal convections in the across-arc direction.
Kyushu Subduction Zone	Hata et al. (2015), Hata and Uyeshima (2015)	Network-MT data, 72 dipoles, Modified 3D data-space OCCAM inversion, Quantitative estimation of temperature and melt fraction distributions in upper mantle	<10	Fore-arc: >1000 Back-arc: ~10	PSP: ~1000 EUP: 10–100	Different conductive anomalies indicate either slab-derived aqueous fluid and/or partial melt beneath the volcanic and non-volcanic regions; Relative contribution of slab-derived fluids to the magmatism vary spatially.
Taiwan Orogen	Bertrand et al. (2009, 2012)	3 MT profiles, 82 stations, 2D NLCG inversion	1–10	PSP: ~1000 EUP: 10–100	PSP: ~1000 EUP: ~100	Deeply extended conductor beneath south and central Taiwan represents fluids generated in thickened crust through metamorphism; Pervasive conductors beneath northern Taiwan suggest the absence of EUP, which is likely removed by slab break-off; all features are consistent with thick-skinned lithospheric deformation.

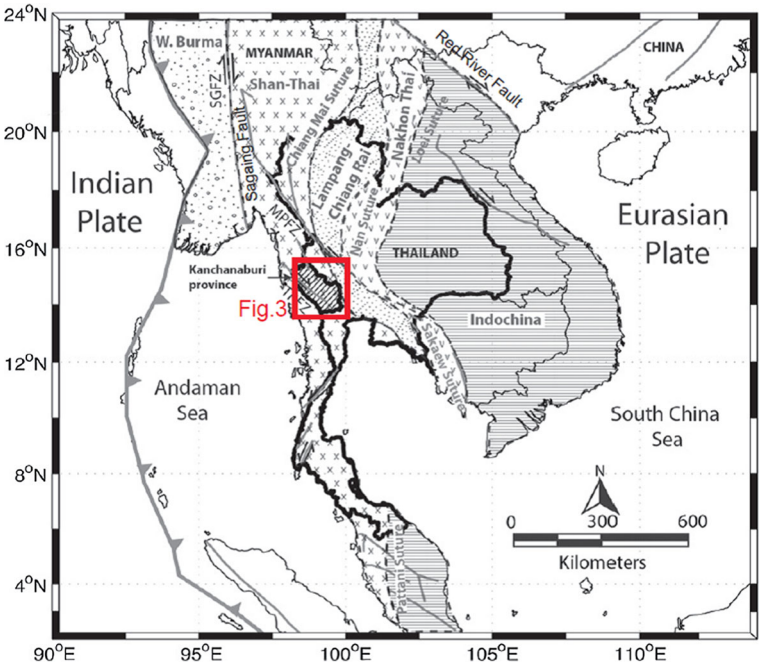

Fig. 2 Simplified tectonic map of Indochina (from Boonchaisuk et al. 2013)

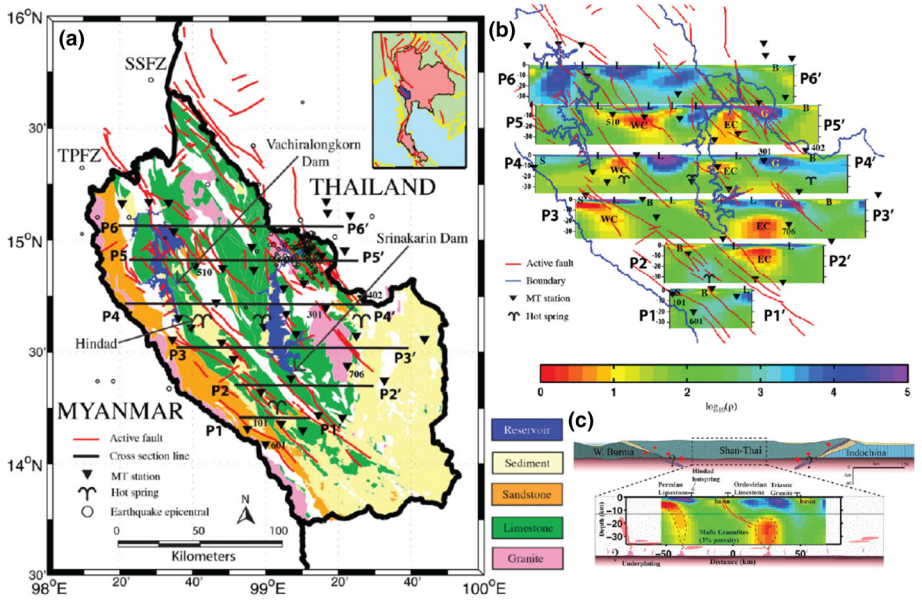

Fig. 3 **a** MT station layout map. **b** Selected vertical slices extracted from the 3-D inversion model. **c** Schematic interpretation of the P3–P3′ line (from Boonchaisuk et al. 2013)

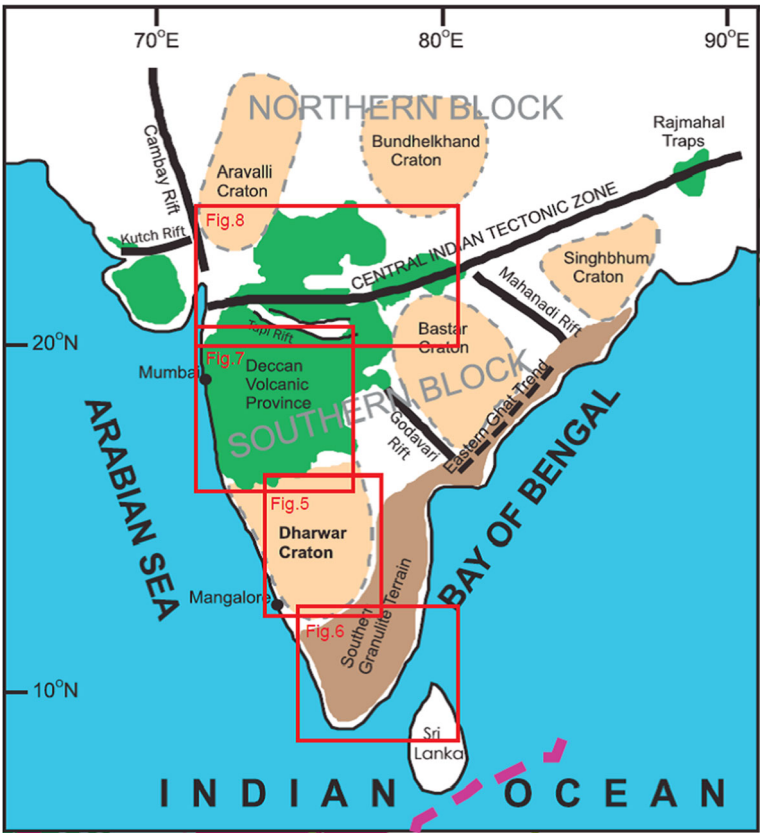

Fig. 4 Simplified tectonic map of the Indian subcontinent (from Abdul Azeez et al. 2015)

Bundelkhand, and Aravalli cratons (see Fig. 4), and has been affected by several major tectonothermal events since its stabilization during the late Archean/early Proterozoic (Abdul Azeez et al. 2015). The geodynamic processes associated with these events rejuvenated many of the Proterozoic mobile belts that created the cratonic units of India and resulted in widespread magmatism. The case studies discussed in this section cover the following four tectonic units of the Indian subcontinent: the Dharwar craton (DC), the Southern Granulite Terrain (SGT), the Deccan Volcanic Province (DVP), and the Central Indian Tectonic Zone (CITZ) (red rectangles in Fig. 4). In a previous review by Harinarayana (2007), the crustal electrical structure of these four tectonic units has been compared and discussed in detail, based on earlier studies. In this review, I will mainly focus on more recent case studies.

2.2.1 Dharwar Craton

As the largest Archean craton of the Indian peninsula, the Dharwar craton includes some of the oldest basement rocks exposed on Earth, with ages over 3.0 Ga, making it one of the most significant cratonic regions of the world. The lithospheric electrical structure of the Dharwar craton has been investigated in several MT studies. Gokarn et al. (2004) obtained

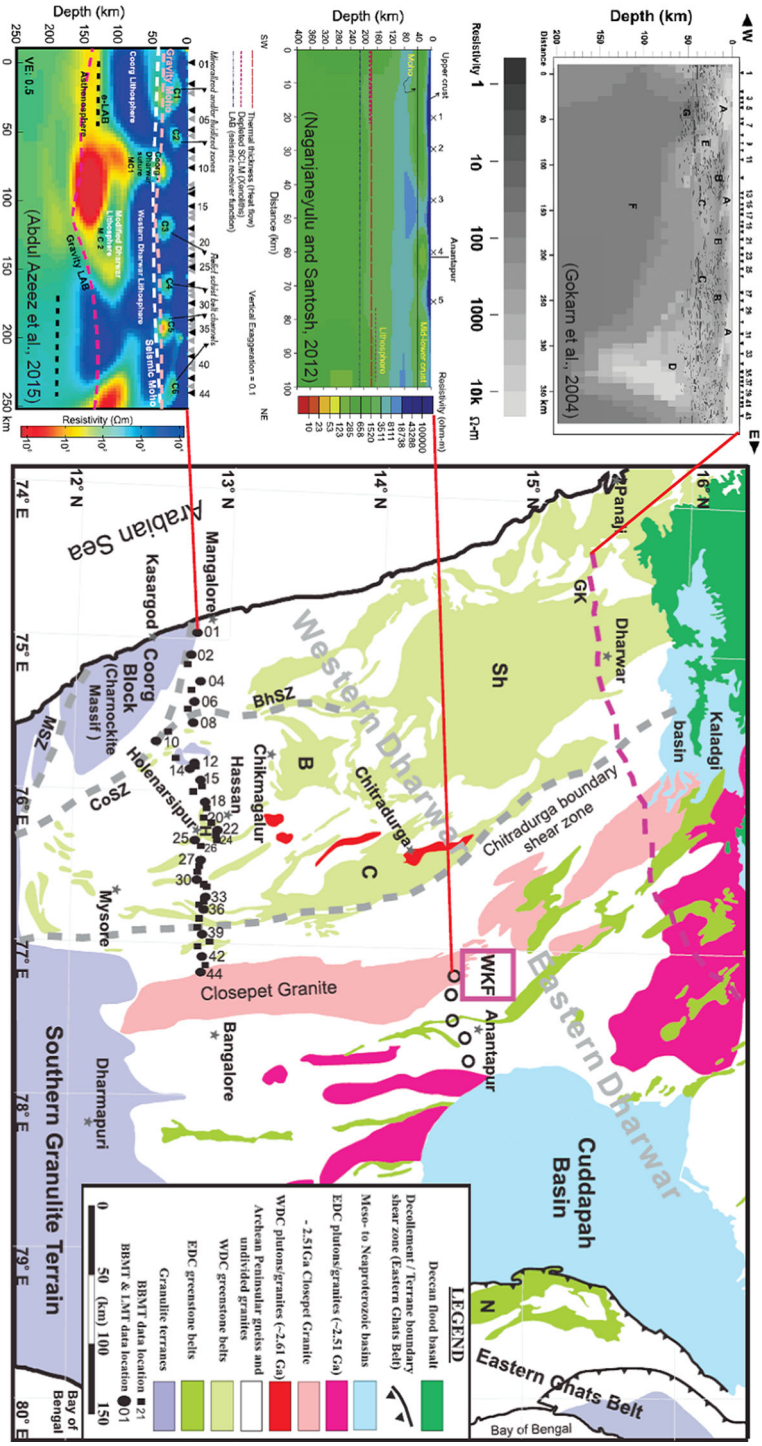
(Gokarn et al., 2004)
(Nagaanjaneyulu and Santosh, 2012)
(Abdul Azeez et al., 2015)
Depth (km)
Resistivity (Ωm)
Arabian Sea
Mangalore
Kasargod
Coorg Block (Charnockite Massif)
Hassan
Chikmagalur
Chitradurga
Chitradurga boundary shear zone
Western Dharwar
Eastern Dharwar
Sh
B
C
GK
Dharwar
Kaladgi basin
Panaji
BhSz
MSZ
CoSZ
WKF
Anantapur
Closepet Granite
Bangalore
Mysore
Dharmapuri
Cuddapah Basin
Eastern Ghats Belt
Bay of Bengal
Southern Granulite Terrain
LEGEND
Deccan flood basalt
Decollement / Terrane boundary shear zone (Eastern Ghats Belt)
Meso- to Neoproterozoic basins
EDC plutons/granites (~2.51 Ga)
~2.51Ga Closepet Granite
WDC plutons/granites (~2.61 Ga)
Archean Peninsular gneiss and undivided granites
WDC greenstone belts
EDC greenstone belts
Granulite terranes
BBMT data location
BBMT & LMT data location
0 50 (km) 100 150

◀**Fig. 5** Geological map of the Dharwar craton with the MT profile locations (right panel) and the corresponding 2-D inversion models (left panels) modified after (Gokarn et al. 2004; Naganjaneyulu and Santosh 2012; Abdul Azeez et al. 2015). Abbreviations are as follows: WDC, western Dharwar Craton; EDC, eastern Dharwar Craton

the two-dimensional (2-D) electrical structure along a 400 km approximately east–west broadband MT profile across the northern portion of the Dharwar craton. Conductive mantle zones have been identified in the depth range of 80–100 km beneath the western Dharwar craton, which were interpreted as the ductile/convecting asthenosphere underlying the rigid (resistive) lithosphere. Observations of the conductive asthenosphere indicate that it deepens eastward beneath the eastern Dharwar craton, with a maximum depth of approximately 160 km (see the upper left subfigure in Fig. 5). Naganjaneyulu and Santosh (2012) estimated the depth of the LAB beneath the central and eastern parts of Dharwar craton based on a short E–W profile that consists of five broadband MT stations (see middle left subfigure in Fig. 5). Their study suggested a lower limit of 175 km for the LAB depth in the eastern Dharwar craton, confirming that this Archean craton preserved a thick lithospheric root. In a more recent MT study by Abdul Azeez et al. (2015), a 250-km-long MT profile was deployed across the Coorg Block and western Dharwar craton, in the east–west direction. Broadband (BBMT) and long-period MT (LMT) data were jointly recorded to generate a 2-D electrical model that resolves the subsurface structure at the lithospheric scale. A subvertical conductor extending from the lower crust into the upper mantle was identified in the transition zone between the Coorg Block and western Dharwar craton, which is interpreted as the paleo-suture zone between the two Archean terrains. Large-scale conductors were also identified in the upper mantle beneath the western segment of the western Dharwar craton, which may indicate modification of the cratonic lithosphere, while a thick lithosphere ($\sim$190 km) was imaged to be preserved beneath the eastern segment of the western Dharwar craton (see lower left subfigure in Fig. 5).

These three case studies all suggest that the Dharwar craton has a three-layer structure (see Fig. 5; Table 1), which consists of a resistive upper crust (5000 to several tens of thousands of Ωm), a relatively conductive mid-lower crust (several hundreds of Ωm), and a resistive upper mantle that represents the lithospheric root of the Dharwar craton (several thousands to several tens of thousands of Ωm). Conductive anomalies ($\sim$20–100 Ωm) are often observed in the marginal regions of the Dharwar Craton, which indicate the modification of the lithosphere. According to the different LAB depths inferred by these three case studies, the average LAB depth beneath the Dharwar craton is approximately 160–190 km, deepening southward and eastward toward the cratonic interior, and the thickest lithosphere is preserved beneath the eastern segment of the western Dharwar craton ($\sim$190 km).

2.2.2 Southern Granulite Terrain

The Southern Granulite Terrain (SGT) lies to the southeast of the Dharwar craton, along the southeastern margin of the Indian peninsula (see Fig. 4). This terrain represents a unique and one of the largest granulite terrains on Earth, exposing a wide range of deformed and retrograded hard crystalline rocks that record a complex evolutionary history. The 3-D lithospheric electrical structure of this terrain was investigated by Patro et al. (2014) using MT data from two parallel, long transects with a N–S extension (Fig. 6). The 3-D inversion model reflects a highly resistive upper crust (several thousands of Ωm) overlying a moderately resistive lower crust (a few hundred Ωm) and an upper mantle with

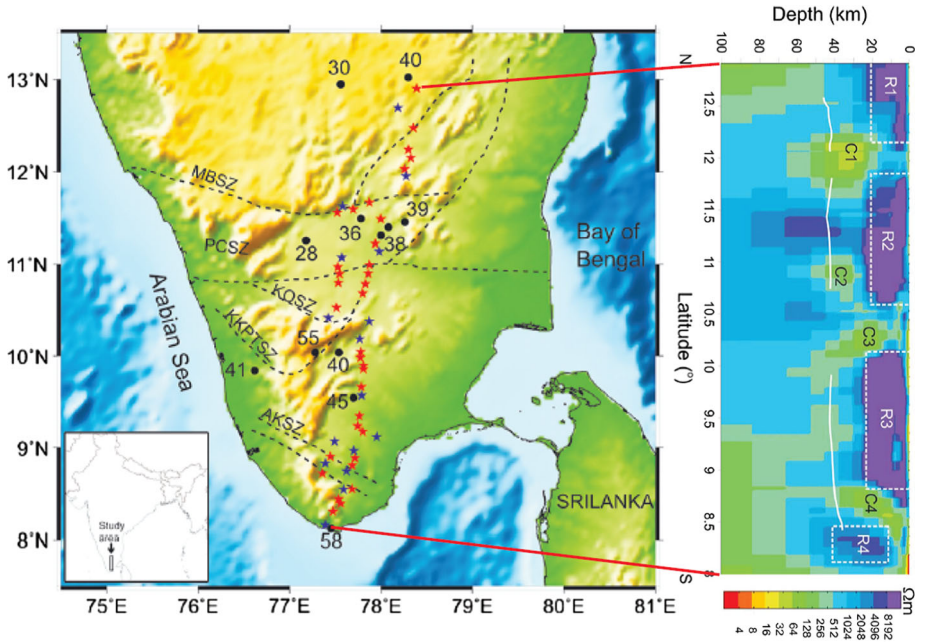

Fig. 6 MT station layout map in the Southern Granulite Terrain (left panel), and a vertical slice extracted from the 3-D inversion model showing the electrical structure beneath the MT profile (right panel) (from Patro et al. 2014). MBSZ, PCSZ, KQSZ, KKPTSZ, and AKSZ are the shear zones. Black dots with numbers indicate the surface heat flow values, in mW/m^2

strong variation in electrical resistivity. Crustal conductors are closely linked to the subduction–collision tectonic processes in the SGT. Their locations provide an important constraint on the boundary between the different geologic units. The northern lithospheric segment is mainly characterized by a thick resistive upper mantle, whereas the southern segment is characterized by predominantly conductive media, suggesting a relatively thinned lithosphere in the southern portion.

2.2.3 Deccan Volcanic Province

The Deccan Volcanic Province (DVP) is located in the northern part of the Dharwar craton (see Fig. 4) and is one of the world's largest LIPs. The 2-D MT modeling results obtained along three profiles in this area (Fig. 7) were examined, integrated, and interpreted with other geophysical data by Patro et al. (Patro et al. 2005; Patro and Sarma 2009). The 2-D inversion models reflect a two-layer lithospheric mantle structure with a high-resistive top layer (several thousands of Ωm) and a conductive bottom layer (a few tens of Ωm to a few hundred Ωm) in the depth range of 50–200 km (see all profiles in Fig. 7). MT models show a good correlation with the velocity structure derived from teleseismic studies, which is inferred to be linked to the compositional changes associated with a depleted lithospheric upper mantle beneath the cold Dharwar craton. A well-defined upper mantle conductor at depths of 80–120 km was identified beneath the DVP (see SP profile in Fig. 7). These features of the study region exhibit several similarities with that of other cratons such as the Slave and Superior cratons in NW Canada. In a recent study, Patro and Sarma (2016)

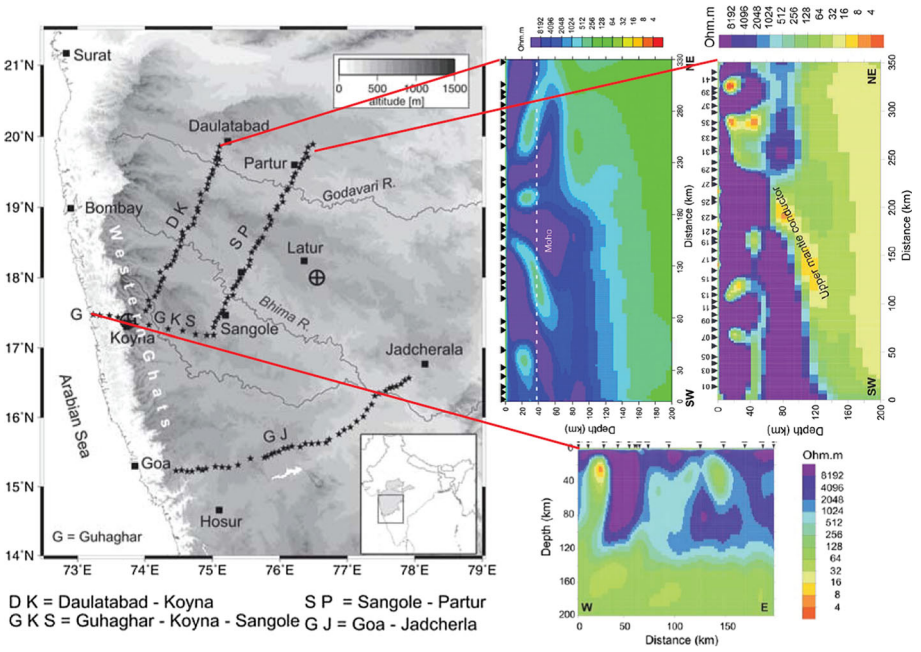

Fig. 7 MT station layout map in the Deccan Volcanic Province (left panel) and the corresponding 2-D inversion models (right panels) (from Patro and Sarma 2009). The GJ profile is the same as in Gokarn et al. (2004) and is shown in Fig. 5

presented a 3-D resistivity model covering the northwestern region of the DVP based on an MT array consisting of 153 sites over a grid with 7- to 8-km spacing. This first 3-D crustal model provides evidence of a large-scale intrusive body that was imaged as a series of major crustal conductors beneath the study area, which provides new insights into the plumbing geometry of the Deccan volcanics.

2.2.4 Central Indian Tectonic Zone

The Central Indian Tectonic Zone (CITZ) is located to the north of the Deccan Volcanic Province. The CITZ was formed in the Paleoproterozoic and is the boundary separating the northern and southern blocks of the Indian peninsula (see Fig. 4); it is recognized as a persistent weak zone, which may have been caused by the Late Cretaceous/early Tertiary Deccan volcanism that was localized in the CITZ. This zone is still tectonically active, as evidenced by sustained levels of seismic activity. Recently, Abdul Azeez et al. (Abdul Azeez 2016; Abdul Azeez et al. 2013, 2017) conducted the first systematic investigation of the resistivity structure of the CITZ using the MT method from west to east across the zone. 2-D resistivity models were generated for five north–south profiles (see Fig. 8) via joint inversion of the transverse electric (TE), transverse magnetic (TM), and tipper data, and the results were integrated with previous MT models in the same region, as well as other geological and geophysical data. The interpretation of these models suggests the existence of widespread conductive zones (10–80 Ωm) in the middle to lower crust. The presence of an interconnected fluid phase and/or hydrous/metallic minerals appears to be the most likely explanation for the elevated conductivity. The presence of fluids may

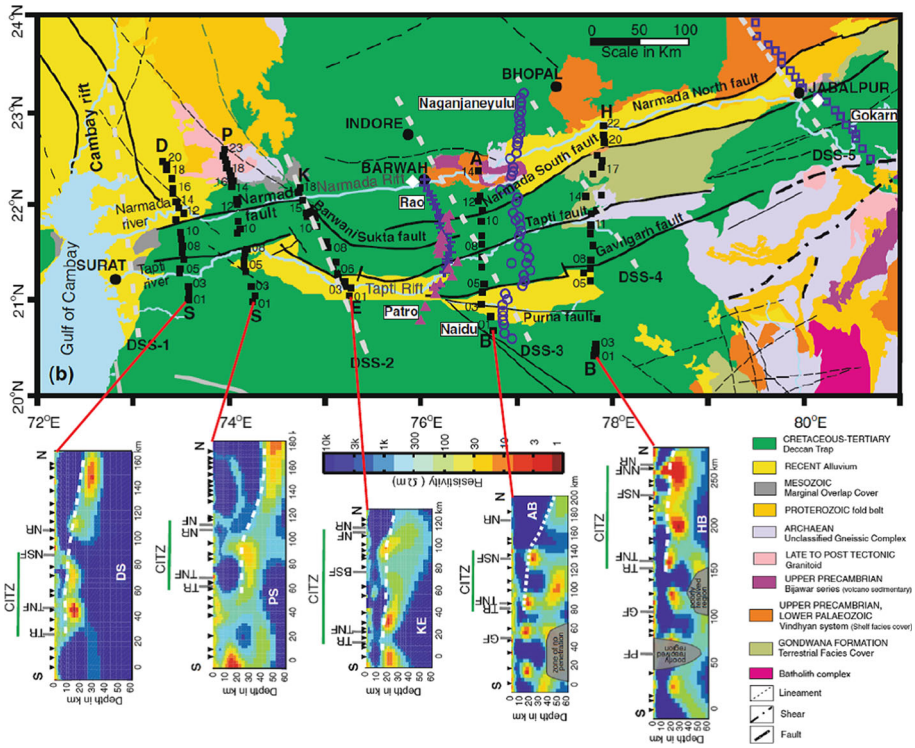

Fig. 8 Geological map of the Central Indian Tectonic Zone with MT profile locations (upper panel) and corresponding 2-D inversion models (lower panels) (from Abdul Azeez et al. 2013). Abbreviations are as follows: PF, Purna Fault; GF, Gavligarh Fault; TNF, Tapi North Fault; BSF, Barwani Sukta Fault; NF, Narmada Fault; NSF, Narmada South Fault; NNF, Narmada North Fault; TR, Tapi River; NR, Narmada River

explain the persistent weakness of the region. A north-dipping conductive layer is observed in the crust within the CITZ, which is consistent with the geometry of the seismic reflectors. This result supports the hypothesis of a northward polarity of the subduction process associated with the formation of the CITZ.

2.3 North China

The North China Craton (NCC) is composed of the Eastern Block, the Western Block (a.k.a. the Ordos Block), and the Trans-North China Orogen (TNCO) (see Fig. 9). The TNCO contains primarily igneous rocks of Paleoproterozoic age. The Western Block is generally considered the oldest and most stable part of the Craton and contains some of the oldest rocks in Asia. The Eastern Block is unusual in that it underwent severe crustal thinning that began in the Mesozoic, and the crustal thickness of this region was reduced from 200 km to as little as 80 km.

In an earlier 2-D MT survey across the TNCO and the Eastern Block, Wei et al. (2008) discovered that the upper mantle beneath the Eastern Block exhibits a widespread, elevated conductivity and that the lithosphere thickness is approximately 50–80 km, strongly suggesting lithospheric thinning of the Eastern Block. By contrast, a large-scale resistor

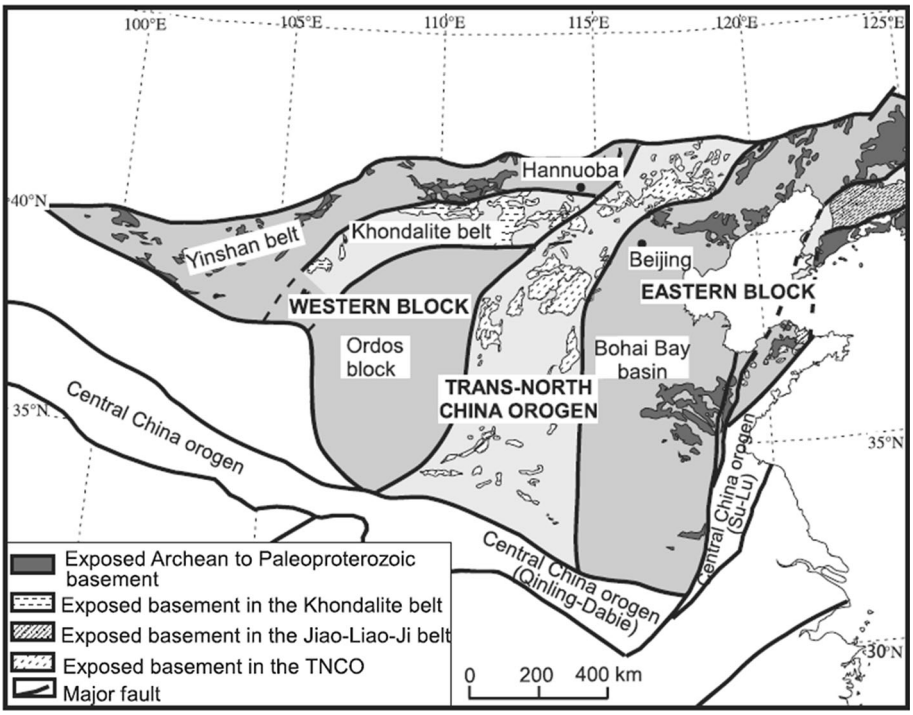

Fig. 9 Simplified tectonic map of the North China Craton (modified after Zheng et al. 2009)

was identified in the upper mantle beneath TNCO, corresponding to the mountain root. Recently, new MT investigations focused on the TNCO have discovered more localized conductors in the lower crust and upper mantle beneath the TNCO and eastern margin of the Ordos Block (Yin et al. 2016, 2017; Zhang et al. 2016), implying that the lithospheric electrical structure of the TNCO is complex and 3-D in nature.

For the Ordos Block, in recent years, a high-resolution 3-D electrical resistivity model was obtained (Dong et al. 2014) by using high-quality LMT data acquired under the auspices of the SinoProbe project (Dong et al. 2011, 2013; Qiu 2013). Contrary to what is expected for a stable cratonic block, a prominent lithospheric conductive complex was observed, which extends from the upper mantle to the mid-to-lower crust beneath the northern part of the Ordos Block and is geoelectrically distinct from that beneath the stable middle and southern Ordos Block (see Fig. 10). By elimination and through consideration of the coincident velocity anomaly, it is suggested that the reduced resistivity may result from a sulfide-related mechanism. The abnormally conductive structure may result from upwelling of the mantle material in the mid-to-late Mesozoic beneath the northern margin of the Ordos Block. Together with the previous seismic studies, it is proposed that the northern margin of the Ordos Block may have experienced regional modification and lithospheric thinning in the destruction process of North China Craton during the late Mesozoic.

Further research investigating the electrical structure in the mantle transition zone beneath the North China Craton was conducted by Xu et al. (2015) using the Geomagnetic Deep Sounding (GDS) method. In their study, 14 geomagnetic stations in North China with

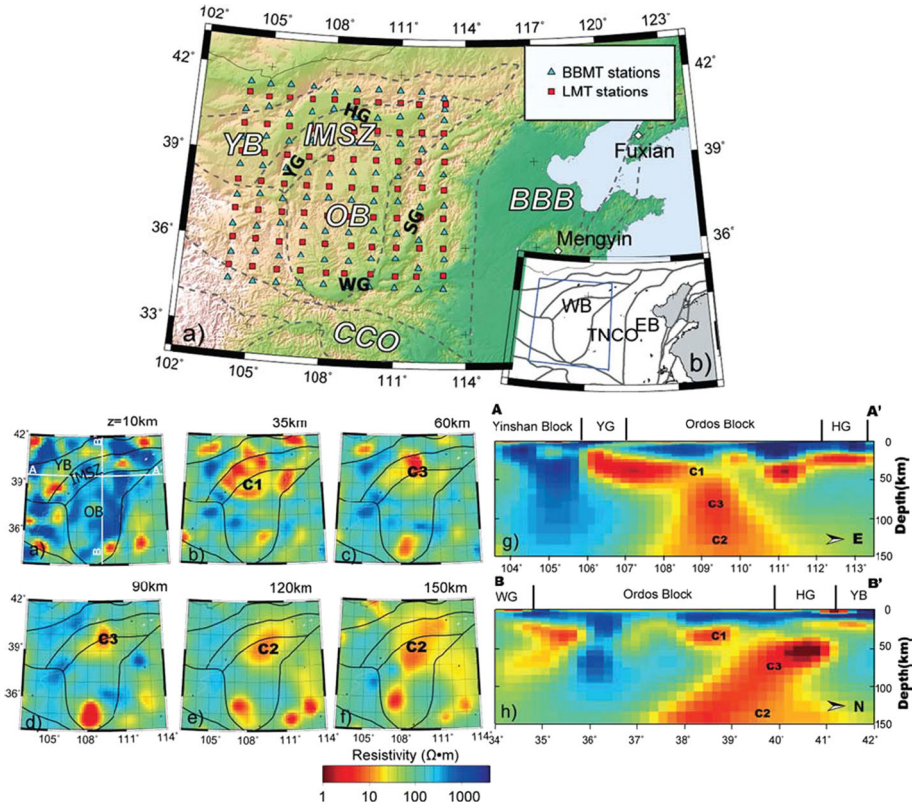

Fig. 10 MT station layout map over the Ordos Block (upper panel) and the horizontal and vertical slices extracted from the 3-D inversion model (lower panel) (from Dong et al. 2014). Abbreviations are as follows: OB, Ordos Block; YB, Yinshan Block; BBB, Bohai Bay Basin; IMSZ, Inner Mongolia Suture Zone; CCO, Central China Orogen; YG, Yinchuan Graben; HG, Hetao Graben; SG, Shanxi Graben; WG, Weihe Graben; WB, Western Block; EB, Eastern Block; TNCO, Trans-North China Orogen

long-period observation data were used to obtain the electrical structure below the lithosphere, particularly in the mantle transition zone (Fig. 11). The GDS response in the period range of $10^5 \sim 10^7$ s was obtained and transformed into an equivalent scalar MT transfer function, which was subsequently inverted with the Occam algorithm to generate smooth one-dimensional (1-D) conductivity models at each station. The inversion models suggest that the conductivity of the mantle transition zone beneath the Eastern Block is $2 \sim 5$ times higher than that of the Ordos Block, which might be associated with the subduction of the Pacific Plate. It should be noted that long-term monitoring methods, such as magnetovariation (GMV) and GDS, are of great significance, as they could not only bring valuable information about much deeper earth than the MT method, but also detect secular variations of the Earth's apparent resistivity (Petrishchev and Semenov 2013).

2.4 South China

The region of South China mainly consists of the Yangtze block in the northwest, the Cathaysia block in the southeast, and the Jiangnan orogen in between these two major

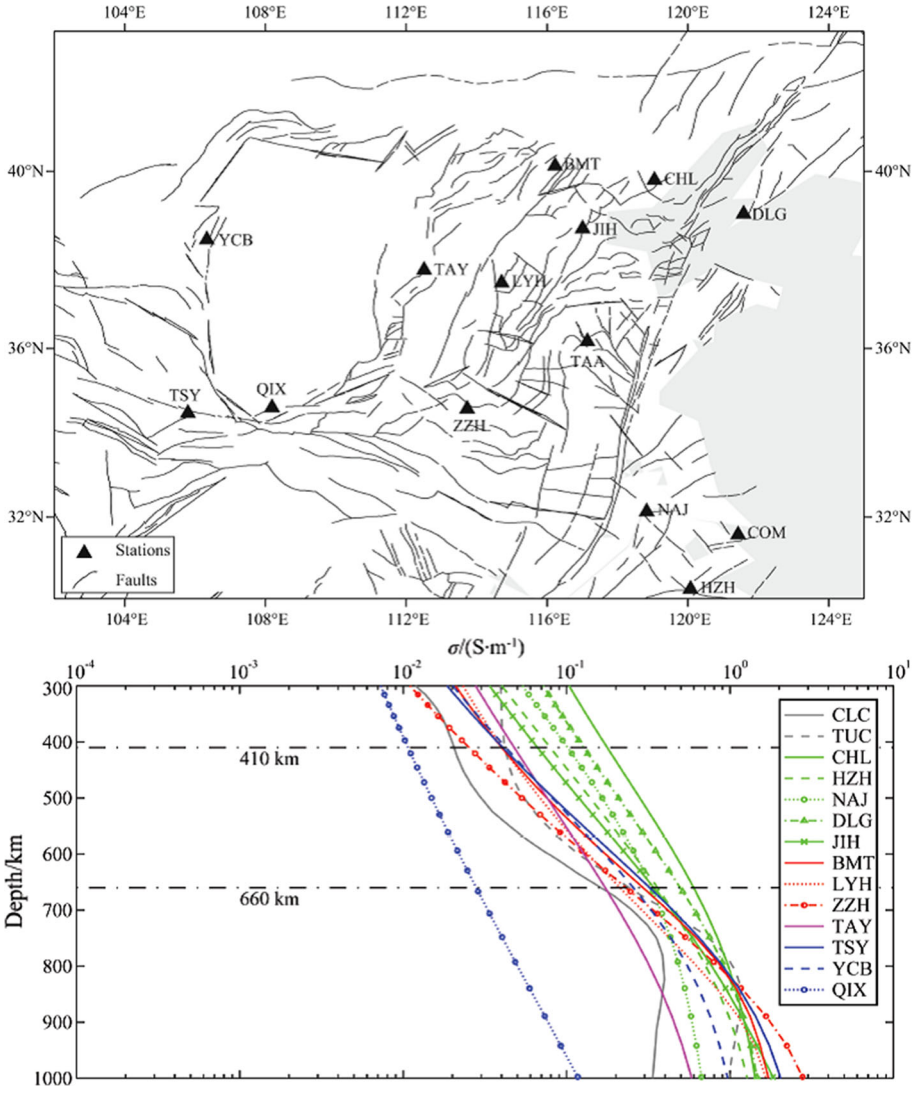

Fig. 11 Geomagnetic station layout map for North China (upper panel) and the corresponding 1-D inversion curves (lower panel) (from Xu et al. 2015). For comparison, curves CLC and TUC are from the Carty Lake in the Canadian Shield and Tucson in the southwestern USA

Precambrian continental blocks (see Fig. 12). The Yangtze block is generally considered a cratonic block of Archean age, whereas the age of the Cathaysia block is still debated due to its poorly exposed basement. In general, the South China block is considered to have formed through the amalgamation of the Yangtze block and the Cathaysia block along the Jiangnan orogen. However, given its long history of evolution, the South China block exhibits very complicated structural patterns, and it is still controversial in many detailed aspects. Since the Mesozoic, the region of South China has been constrained by three major convergent tectonic domains, which are the westward subduction of the Pacific Plate, the northward subduction of the India Plate beneath the Eurasian Plate, and the

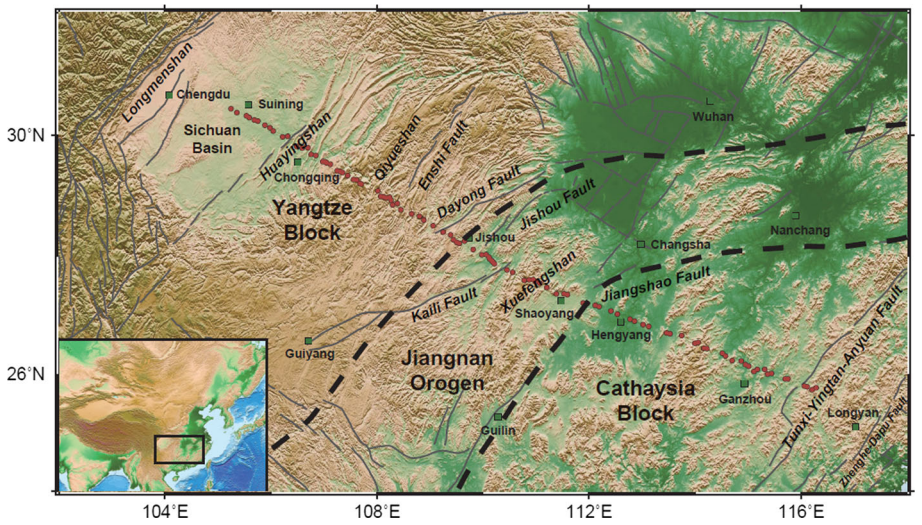

Fig. 12 MT station layout map for South China (from Zhang et al. 2015a)

convergence between the North and South China blocks. Within this compressional tectonic domain, the structures in South China are primarily characterized by shortening, thrusting, and decollement. The study of the tectonics in this region is of great significance given its important role in understanding the formation of the Asian continent.

Under the auspices of the SinoProbe Project, a 1200-km-long magnetotelluric (MT) profile across the major parts of South China was completed, comprising 99 BBMT stations (see Fig. 12). TE and TM data were jointly inverted using the nonlinear conjugate gradient (NLCG) algorithm of Rodi and Mackie (2001) to produce a 2-D electrical structure model along the profile (see Fig. 13) (Zhang et al. 2015a). The 2-D inversion result shows that the lithospheric electrical structure of South China is generally resistive, which corresponds to the basic feature of a stable Precambrian tectonic setting. The electrical structure along the profile could be generally described as three resistive bulks (R1, the western Yangtze block; R2–R4, the Jiangnan orogen; and R5–R7, the Cathaysia block) separated by two major conductors (C1, the eastern Yangtze block; and C2, the Jiangshao fault). The resistive western Yangtze block represents the stable cratonic region of Archean age, whereas the electrically conductive eastern Yangtze block is characterized

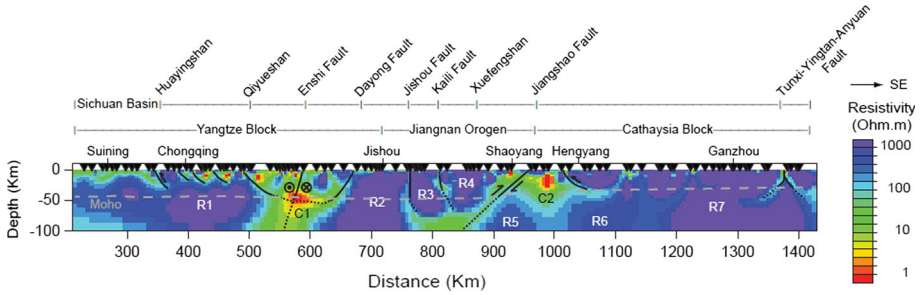

Fig. 13 Tectonic interpretation of the 2-D inversion model across South China (from Zhang et al. 2015a)

by the lithospheric shearing of a strike-slip fault system and the extension that is probably caused by slab rollback in the mantle transition zone at the frontal edge of the flat-plate subduction. The west-dipping conductor C2, which is located directly beneath the Jiangnan orogen, represents the paleo-suture between the Yangtze and Cathaysia blocks. The Jiangnan orogen is a typical intra-continental orogen, which is formed within a continent, far from active plate margins. This feature suggests that the intra-continental orogens are generally formed along paleo-sutures, where the lithosphere is relatively weak and easy to be deformed.

2.5 Comparison and Summary of the Major Continental Blocks

The major continental blocks discussed in this section represent some of the most stable regions of the Asian continent. By comparing these regions, we can see that most of the continental blocks exhibit a three-layer structure with a resistive upper crust and upper mantle (hundreds to tens of thousands of Ωm) above and below a relatively conductive mid-lower crust (tens to hundreds of Ωm), respectively (see Table 1). Two exceptional cases are also discussed; the first is Indochina, for which the upper mantle structure was not resolved due to a limited penetration depth, and the second is the Yangtze craton of South China, where the upper crust is covered by thick sediments of the Sichuan Basin that are relatively conductive (several tens of Ωm, see Fig. 13).

In general, the distribution of the mid-lower crustal conductors is localized in the stable continental blocks, and their locations are strongly correlated with paleo-sutures or fossil subduction zones. For example, large-scale conductors have been observed in the lower crust and upper mantle beneath paleo-suture zones in both the Dharwar craton and Ordos Block, which indicate modification of the marginal cratonic lithosphere in western Dharwar and northern Ordos (see Figs. 5 and 10).

Although the LAB depth was not determined in all cases due to limited skin depth, it can still be seen that most of the major continental blocks have preserved a thick, resistive (several thousands to several tens of thousands of Ωm) lithospheric root in their core regions. In the Dharwar Craton, the average LAB depth is approximately 160–190 km. In the North China Craton, the LAB depth is approximately 130 km in southern Ordos, whereas in the northern part of Ordos, the lithosphere is modified, as evidenced by a large-scale conductor extending from the lower crust into the upper mantle (see profile B–B' in Fig. 10). In the Yangtze craton in South China, the lithosphere is at least 100 km thick, although its lower boundary was not resolved (see Fig. 13).

The case studies discussed above reveal several basic features of the constituent nucleus of Asia. However, these studies only represent a small portion of the Asian continent. As shown in Fig. 1, a much larger portion of the Asian continent has active orogenic belts and subduction zones. The lithospheric electrical features of these regions are discussed in the following sections.

3 Lithospheric Electrical Structure of the Major Orogenic Systems

3.1 Central Asian Orogenic System

In many parts of Asia, mountain building and the associated crustal exhumation/denudation are still very active as a result of continuous India–Asia convergence (e.g., growth of

the Tibetan Plateau and development of the Central Asian Orogenic Belt) or subduction of the Pacific at the eastern margin (e.g., Japanese Islands) (Safonova and Maruyama 2014). Collisions between major continental blocks formed most of the orogenic belts of Asia. Episodes of collisions between the Siberian, Tarim, and North China cratons resulted in the closure of the Paleo-Asian Ocean in Carboniferous-Permian time. These collisions and oceanic closures formed the Central Asian Orogenic Belt (CAOB). The CAOB is generally recognized as a major site of Phanerozoic juvenile crustal growth and is a typical accretionary orogeny, which is created through the collision and suturing of partially juvenile crustal blocks (e.g., ophiolites, continental arcs, and oceanic plateaus) as well as reworked older crust to continental crust at sites of continuing oceanic plate subduction. The MT method has been effectively used to investigate the lithospheric electrical structure of this large-scale orogenic system. In this section, three case studies will be introduced; one case study is focused on the western segment of the CAOB, and the other two case studies are focused on its eastern segment.

3.1.1 Western Segment

In the western segment of the CAOB, a 182-km-long MT profile comprising 60 BBMT stations was deployed in the western Junggar area of NW China (see Fig. 14a) (Xu et al. 2016a). This region is generally recognized as an accretionary collage bounded by the Junggar Basin to the east, the Tacheng Basin to the west, the NW Tianshan orogen to the south, and the CAOB to the north. Off-diagonal impedances were inverted using the ModEM code (Egbert and Kelbert 2012; Kelbert et al. 2014) with the NLCG algorithm. A vertical slice extracted from the 3-D inversion model beneath the MT profile was interpreted in combination with geological and geophysical observations, mineral physical experiment, and geodynamic modeling results (see Fig. 14b). The MT transect suggests a fossil Late Carboniferous intra-oceanic subduction system with a SE to NW polarity beneath the western Junggar accretionary collage and western Junggar Basin. The preservation of this fossil subduction zone can be ascribed to the lack of subsequent tectonothermal events, which is supported by stable and continuous sedimentary strata in the western Junggar Basin.

3.1.2 Eastern Segment

In the eastern segment of the CAOB, two MT transects were completed in recent years across the northeastern margin of the North China Craton (Dong et al. 2015) and the Great Xing'an Range (GXR) (Liang et al. 2015; Xiong et al. 2015) (see Figs. 15, 16). A 2-D inversion model across the northeastern margin of the North China Craton reveals a northwest dipping crustal conductor beneath the Solonker suture, which is identified as the suture zone between the Siberia and North China Cratons (Fig. 15). The CAOB is characterized by a relatively thick lithosphere with an upper mantle resistivity in the range of 300–1000 Ωm. Following the method proposed by Rippe et al. (2013), this feature can be interpreted quantitatively, and the resistivity value can be explained by an elevated concentration of H+(800–1000 wt ppm). By contrast, the lithosphere beneath the northeastern North China Craton is revealed to be thin and less resistive (<100 Ωm). Partial melts, or other conducting phases are needed to explain this feature. Furthermore, significant lateral variation in the electrical resistivity of the lithosphere indicates that the modification of the lithosphere associated with the craton destruction is spatially non-uniform. In the 2-D electrical model across the GXR (Fig. 16), the upper crust of the GXR is characterized by

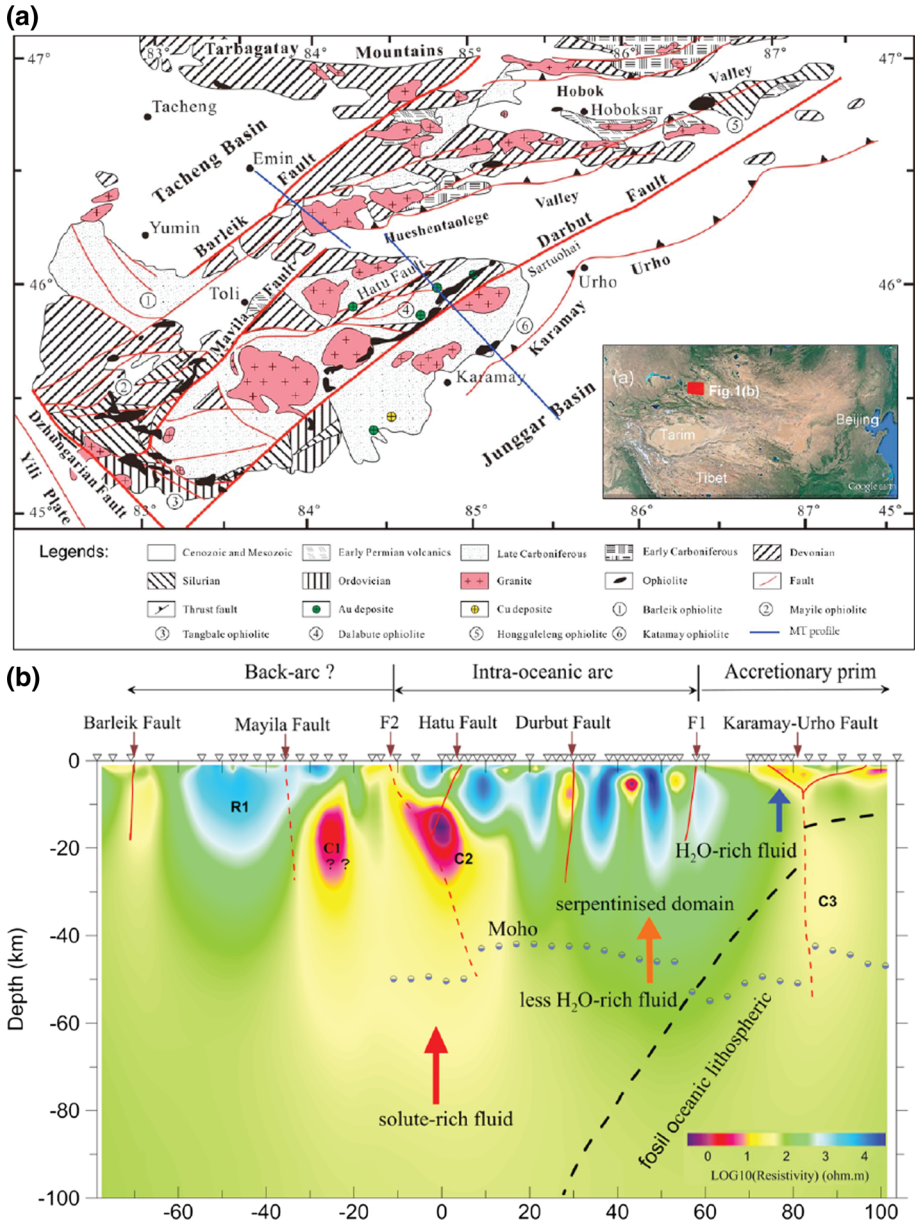

Fig. 14 **a** Simplified tectonic map of western Junggar showing the locations of MT profiles. **b** Vertical slice extracted from the 3-D inversion model showing the electrical structure beneath the MT profile (from Xu et al. 2016a)

an overall high resistivity with some localized conductors in the mid-lower crust. This feature may imply that the upper crust is mainly composed of volcanic rocks and that hot and weak materials exist in the mid-lower crust. A large-scale resistor is observed in the lithospheric mantle, implying that the lower crust of the GXR may have experienced

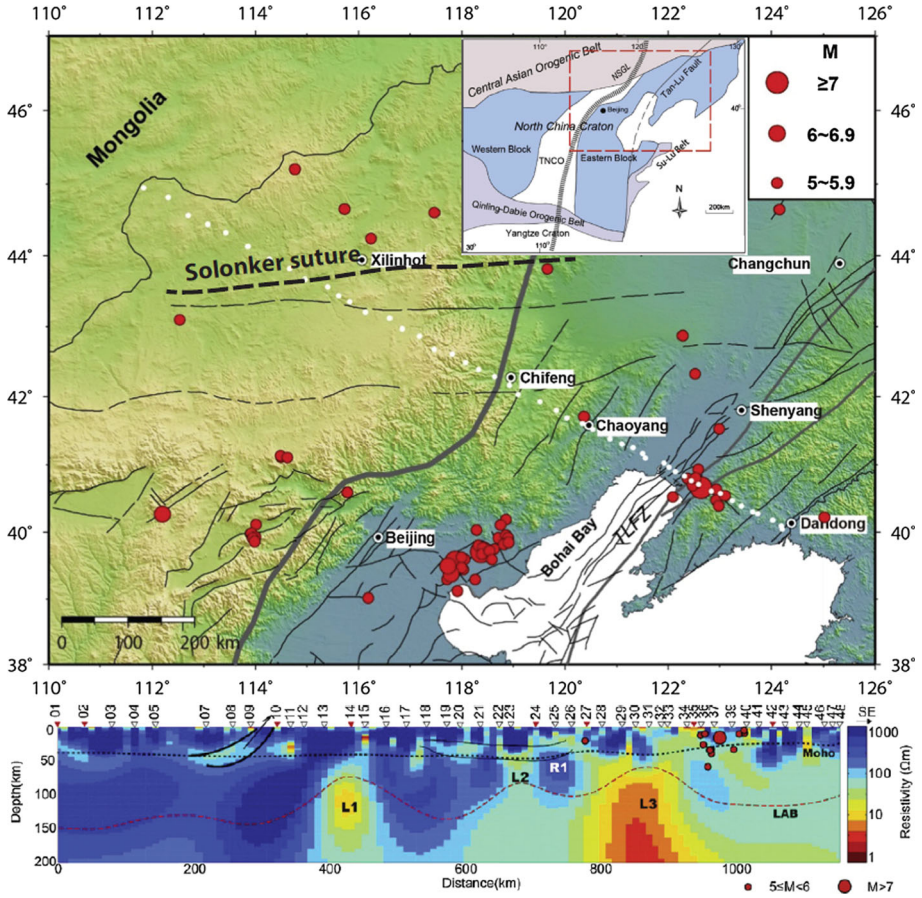

Fig. 15 MT station layout map in the NE margin of the North China Craton and the tectonic interpretation of the 2-D inversion model (from Dong et al. 2015)

delamination, which is a common feature in the eastern segment of the CAOB. A lithospheric west-dipping conductive zone is revealed between the GXR and the Songliao Basin, which is inferred as the residual convergence zone in the form of soft collision.

3.2 Tethyan Orogenic System

The Tethyan orogenic system is a typical collisional orogeny, which formed during the collision between several cratonic segments of the lithosphere as the Tethys Ocean and its branches closed (Proto-Tethys, Paleo-Tethys, Meso-Tethys and Neo-Tethys). This large-scale orogenic system is still active and primarily influenced by the Arabia–Asia collision in the west and the India–Asia collision in the east (Yin 2010). When the direction of colliding plates is orthogonal, the crust is greatly thickened, and thrusting, metamorphism, and partial melting may rework the colliding blocks and produce juvenile crust during collisional orogeny. The following case studies discussed in this section are organized according to their locations in the Tethyan orogenic system: from the western extent to the eastern extent. As a key part of this review, in this section, I will also introduce a three-

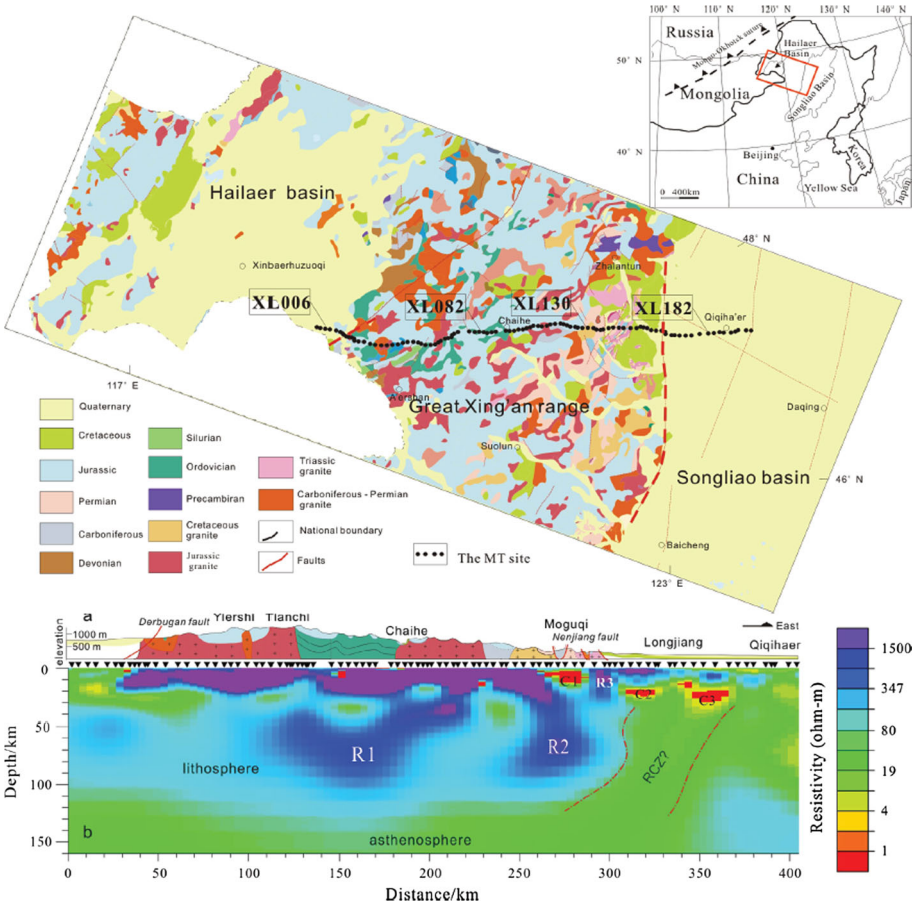

Fig. 16 MT station layout map in the Great Xing'an Range and the tectonic interpretation of the 2-D inversion model. RCZ: Residual convergence zone (from Liang et al. 2015 and Xiong et al. 2015)

dimensional (3-D) model of the lithospheric electrical structure of a large portion of the Tibetan Plateau, in detail.

3.2.1 North and East Anatolian Faults

The Arabian plate is located in the Middle East in western Asia and is a continent block that was separated from Africa by the Red Sea Rift approximately 25 million years ago in the Oligocene. Since then, the northward drift of the Arabian Plate (together with the Indian Plate) lead to the closure of the Tethys Ocean and collision with the Eurasian Plate. The indentation of the Arabian Plate caused the extrusion along the North and East Anatolian faults in the west and formation of the Zagros collision belt in the northeast.

The western segment of the Tethyan orogenic system consists of the right-lateral strike-slip North Anatolian fault (NAF) and the left-lateral strike-slip East Anatolian Fault (EAF). They behave as a conjugate system, guiding the extrusion of the Anatolian Block in response to the indentation of the Arabian Plate (see Fig. 17). Previous MT studies have

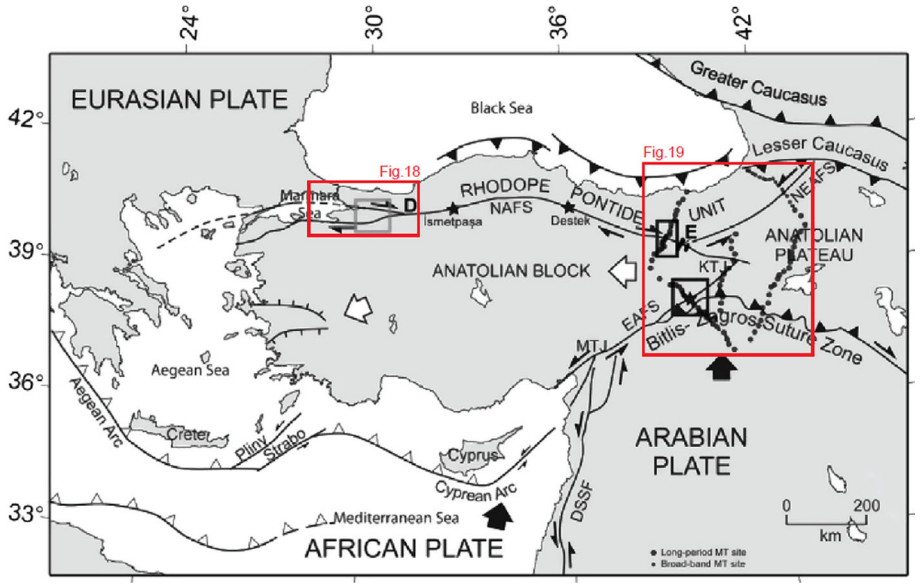

Fig. 17 Simplified tectonic map of Turkey and the surrounding areas (from Türkoğlu et al. 2015)

mainly focused on the western extent of the NAF (Kaya et al. 2009, 2013; Tank et al. 2003, 2005) and eastern extent of the Anatolian Block (Avşar et al. 2013; Türkoğlu et al. 2008, 2015).

2-D resistivity models near the western extent of the NAF indicate the existence of a conductor at a depth of $\sim$10 km with a deeper extension into the upper mantle, suggesting the presence of fluid in the crust and partial melting in the upper mantle (see Fig. 18). The conductor was identified farther to the east along the NAF, suggesting that the electrical characteristics of this fault are continuous from the inland areas into the Marmara Sea (Kaya et al. 2013).

Near the eastern extent of the Anatolian Block, the lithospheric electrical structure is characterized by a lower crust with a low resistivity (fluid rich) underlain by a relatively normal upper mantle (see Fig. 19). The lower crust of the Anatolian Plateau contains areas of very low resistivity that may indicate local accumulations of melt. This area is underlain by an upper mantle with anomalously low resistivity that can be accounted for by an asthenosphere containing a few percent of partial melt. The presence of fluids may sufficiently weaken the crust and mantle to allow lateral flow and may also allow decoupling of the upper and lower portions of the lithosphere (Türkoğlu et al. 2008). In the eastern end, both the NAF and EAF are underlain by a broad low-resistivity zone that extends into the lower crust. By contrast, the resistivity beneath the EAF was much lower than that beneath the eastern part of the NAF (Türkoğlu et al. 2015).

3.2.2 Zagros Collision Belt

The relatively young Zagros collision belt is an active fold-and-thrust belt formed in the foreland of the collision between the Arabian and Eurasian Plates. This belt is approximately 1800 km long and characterized by highly deformed crustal rocks. Recently, Oskooi et al. (2014) presented the first electrical conductivity model across the Zagros

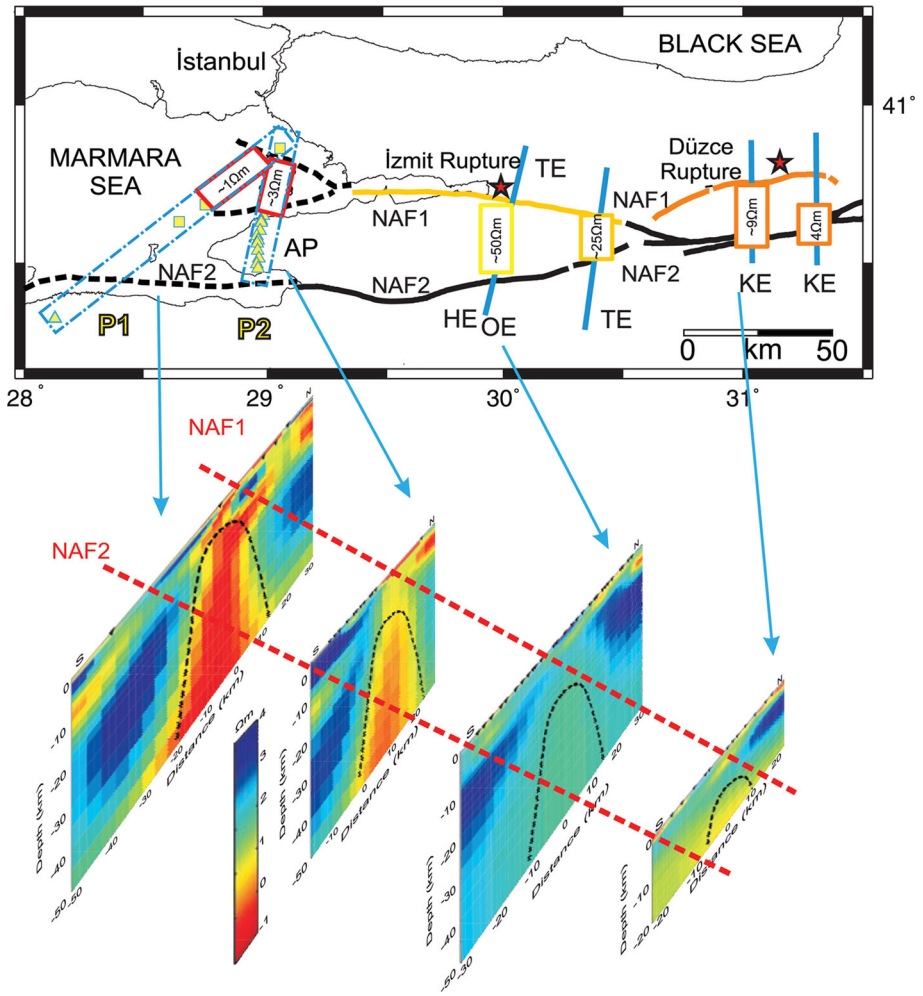

Fig. 18 2-D resistivity models around the western extent of the NAF (from Kaya et al. 2013). Abbreviations are as follows: AP, Armutlu Peninsula; NAF, North Anatolian fault. TE, HE, OE, and KE are the MT profile labels

collision belt based on a 2-D MT transect. The location of this profile and the corresponding 2-D model are shown in Fig. 20. The new MT model reveals a transition belt between the Arabian Plate and the Eurasian Plate. Along the surface trace of the Main Zagros Thrust (MZT, location corresponds to station 31 from the 2-D model in Fig. 20), the transition between the two continents is imaged as a series of conductors and resistors varying both horizontally and vertically with complex geometry. The model also suggests that, in general, the Arabian Plate is more conductive than the Eurasian Plate to depth of 100 km. A 2-D MT study was also conducted at a smaller scale to investigate the ophiolites in the Neyriz area of southwestern Iran within the Zagros fold-and-thrust belt (Oskooi et al. 2015) (see Fig. 21). From the outcome of the 2-D inversion model, the fault plane of the MZT, as well as the border between the ophiolite and radiolarite zones, is clearly imaged as strong resistivity contrasts in the northeastern and southwestern portions

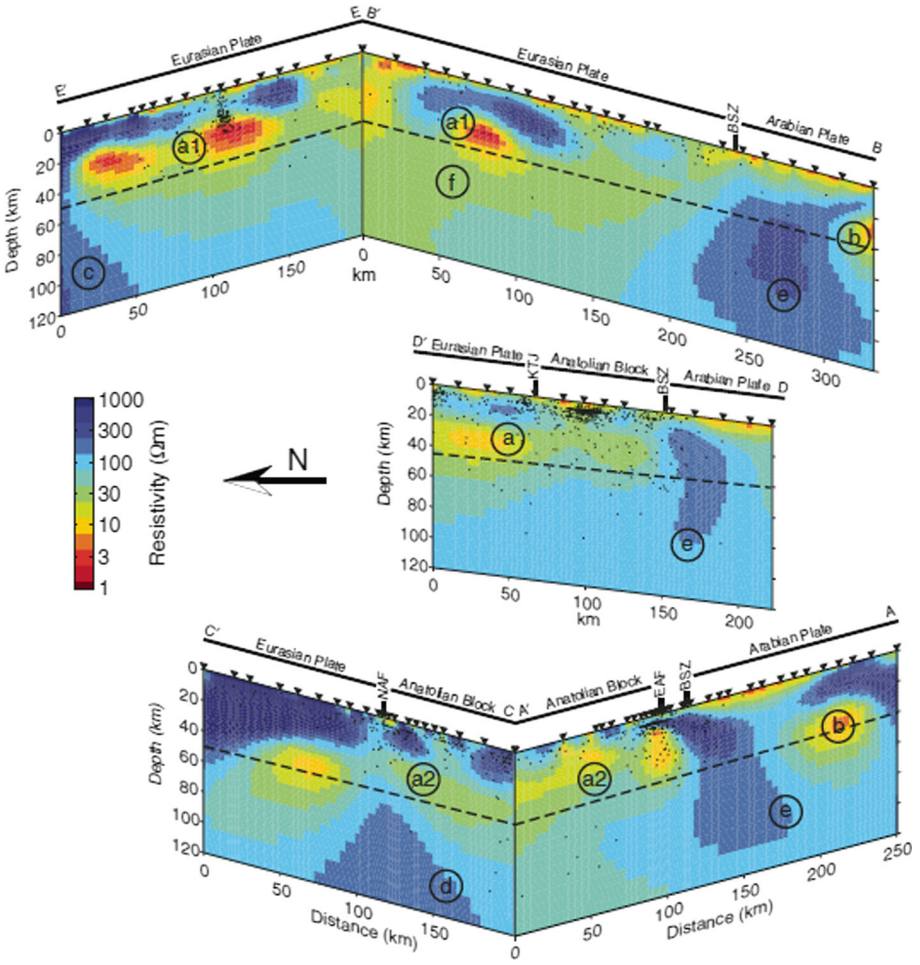

Fig. 19 2-D resistivity models around the eastern extent of the Anatolian Block (from Türkoğlu et al. 2008). Abbreviations are as follows: BSZ, Bitlis suture zone; KTJ, Karlıova triple junction; NAF, North Anatolian fault; EAF, East Anatolian Fault

of the profile, respectively. Meanwhile, the Neyriz ophiolite assemblage (NO) is highly resistive, whereas the Sanandaj–Sirjan metamorphic zone (SSZ) and MZT are more conductive. These results are consistent with the surface geological mapping work in this area.

3.2.3 Oman Ophiolite Suite

On the eastern corner of the Arabian Plate, the Oman ophiolite suite is believed to have formed at the Tethyan spreading center in an obduction scenario, in which the oceanic lithosphere was thrust onto the continental lithosphere. The Samail Ophiolite in north-eastern Oman is generally considered one of the most well-preserved ophiolite exposures on Earth. The MT method was used to investigate the crustal structure across this belt to compare competing emplacement models (Thiel et al. 2009). The 2-D MT profile is

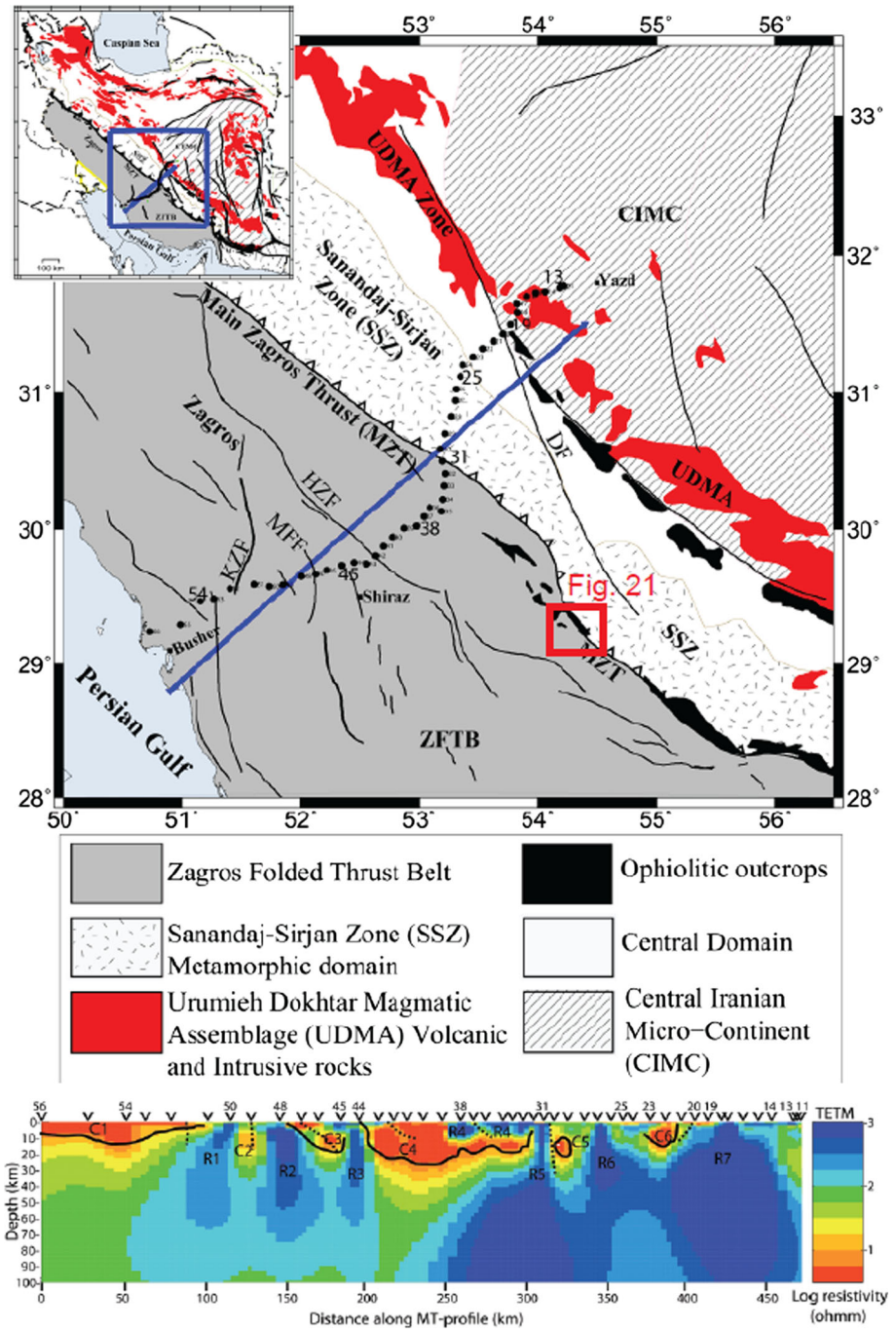

Fig. 20 Map showing the location of the 2-D MT transect across Zagros (upper panel) and the corresponding 2-D resistivity model (lower panel) (from Oskooi et al. 2014)

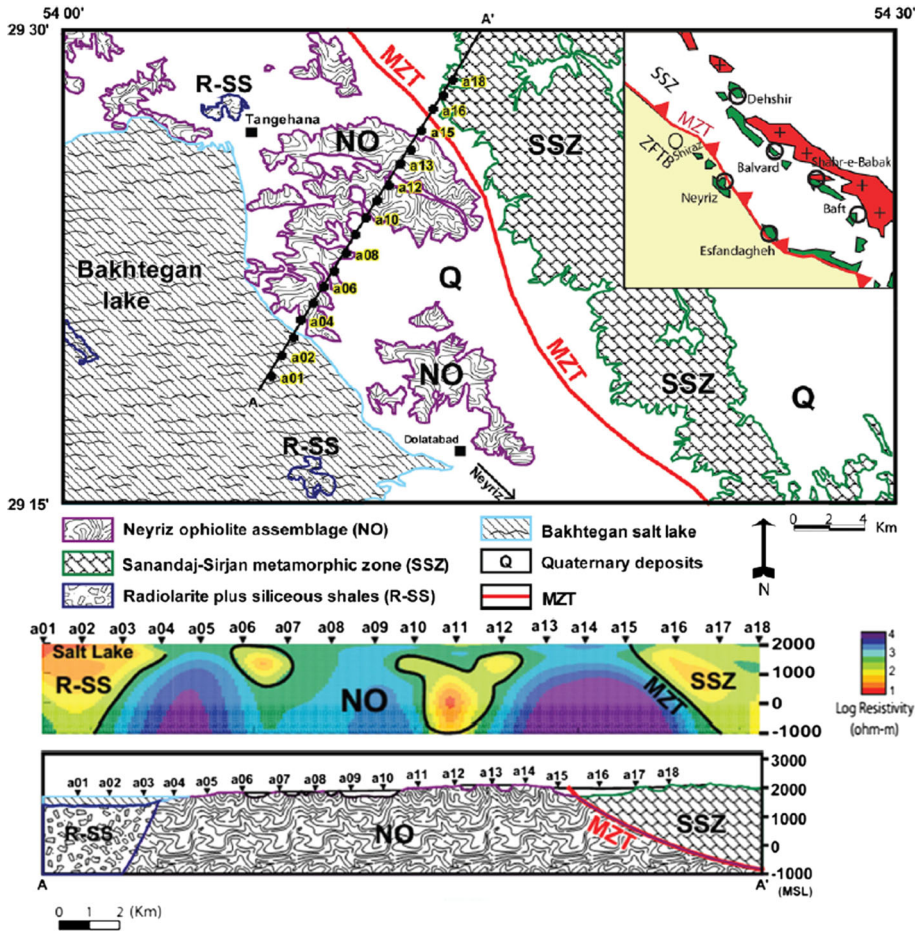

Fig. 21 Geological map of the Neyriz ophiolite belt with MT station locations (upper panel) and the tectonic interpretation of the corresponding 2-D inversion model (lower panel) (from Oskooi et al. 2015). Abbreviations are the same as in Fig. 20

approximately 115 km long and consists of 16 stations (see upper panel of Fig. 22). The major discovery from the resultant 2-D resistivity model (see lower panel of Fig. 22) was that the majority of the resistivity interfaces dip toward the continental margin of the Arabian Plate, which suggests a southwestward underthrusting prior to the ophiolite emplacement. This model agrees with the obduction scenario that involves an early stage of subduction of the oceanic lithosphere beneath the Arabian continental margin, where a major southwest-dipping shear zone is preserved in the crust beneath the Oman Mountains.

3.2.4 Pamir

The Pamir and southern Tian Shan orogenic belts are located at the northwestern corner of the India–Asia collision zone. This region is the best place to study the process of intra-continental collision. Sass et al. (2014) investigated the lithospheric electrical structure beneath this region via a 350-km-long, north–south trending MT profile (see Fig. 23). The

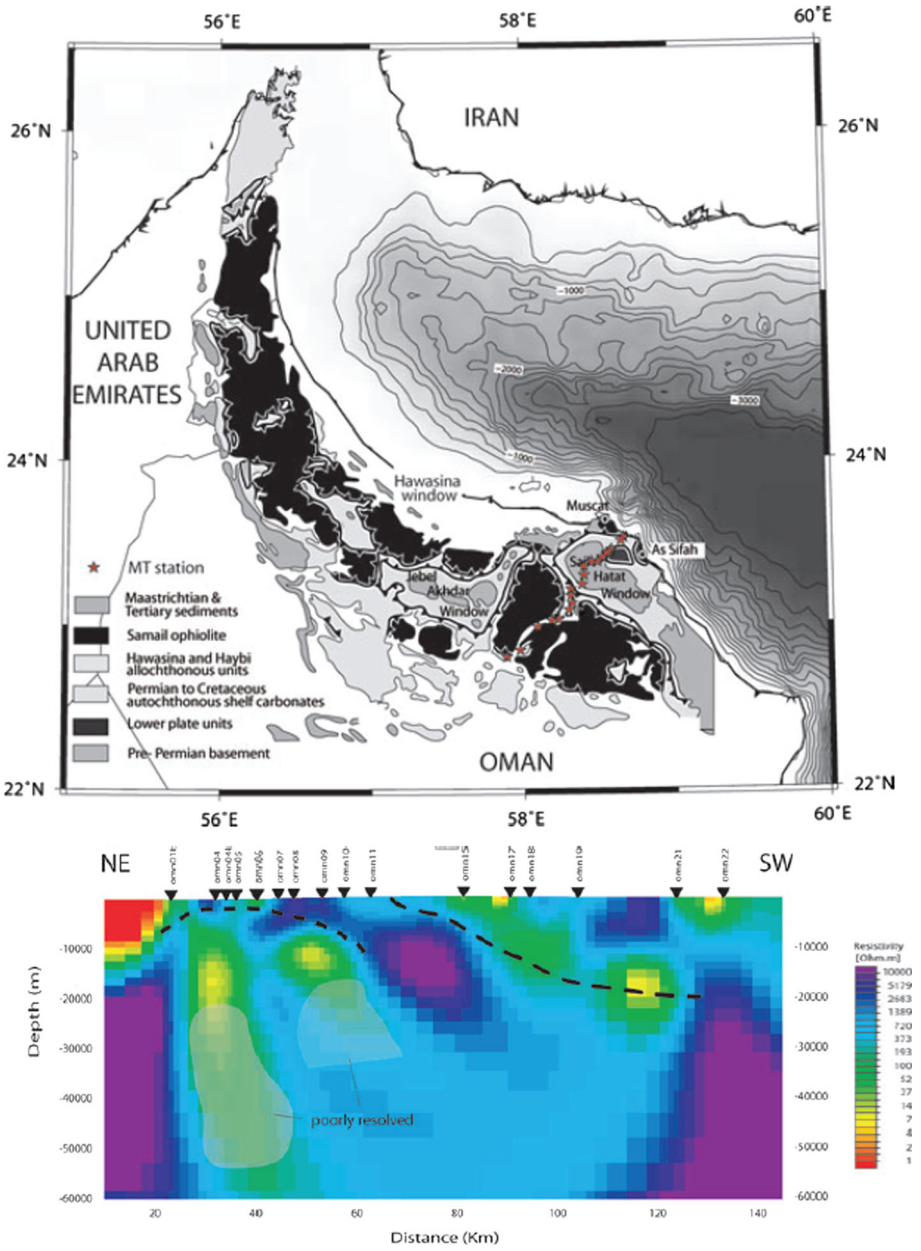

Fig. 22 Simplified geological map with the MT station locations (upper panel) and the 2-D MT model across the Samail Ophiolite in NE Oman (lower panel) (from Thiel et al. 2009)

most intriguing feature revealed by both the 2-D and 3-D inversions is a laterally extended conductive zone below the Pamir Plateau, with resistivities below 1 Ωm, below depth of ~10–15 km. The high conductivity can be explained with the presence of partially molten rocks in the middle to lower crust, possibly related to ongoing migmatization and/or

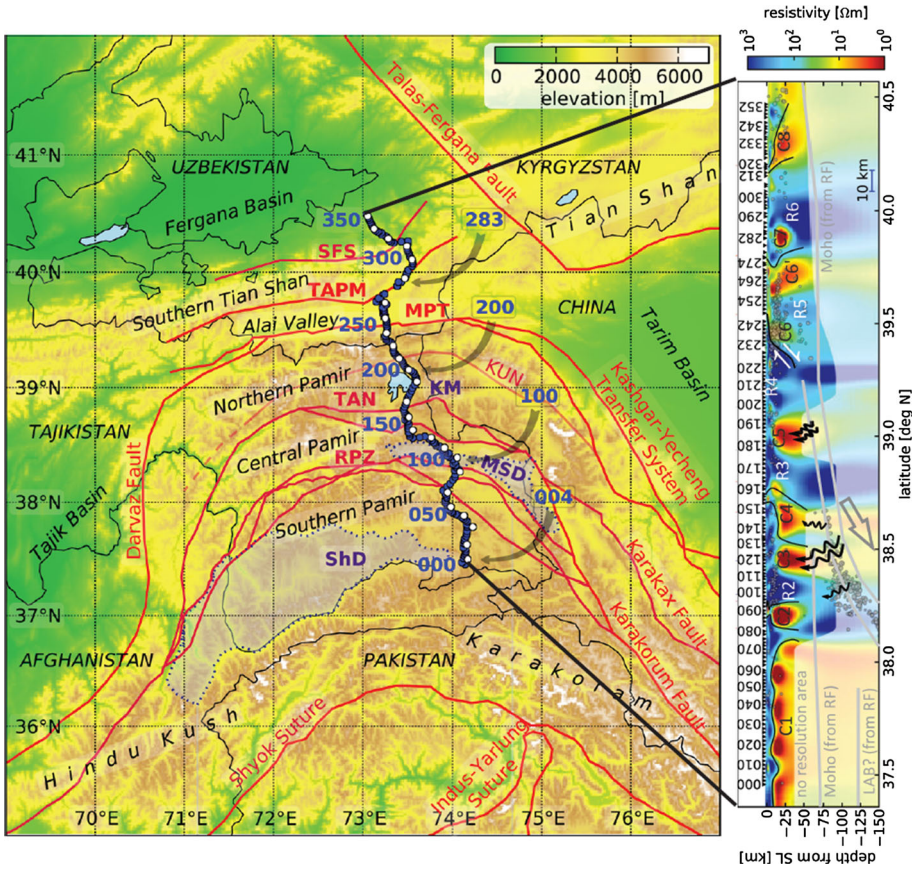

Fig. 23 MT station layout map in the Pamir and Southern Tian Shan orogenic belts (left panel) and the corresponding 2-D resistivity model (right panel) (from Sass et al. 2014). Blue and white dots represent the BBMT and LMT stations, respectively. Abbreviations are as follows: KM, Karakul–Mazar Unit; KUN, Kunlun suture; MPT, Main Pamir Thrust; MSD, Muskol–Shatput Domes; RPZ, Rushan–Pshart suture zone; ShD, Shakhdara dome; SFS, South Fergana Suture Zone; TAN, Tanymas Suture Zone; TAPM, Turkestan–Alai Passive Margin

middle/lower crustal flow underneath the southern Pamir orogenic belt. In the upper crust of the Pamir and Tian Shan orogenic belts, the Paleozoic–Mesozoic suture zones are electrically conductive, whereas the compact metamorphic rocks in the central Pamir belt are highly resistive. Several deeper zones of high conductivity in the middle and lower crust of the central and northern Pamir orogenic belt likely record the fluid released due to metamorphism associated with the active continental subduction/delamination.

3.2.5 The Tibetan Plateau and its Surrounding Regions

The ongoing continent–continent collision between the Indian and Eurasian plates since ~55 Ma has created the spectacular topography of the Tibetan Plateau. However, many first-order questions regarding the mechanisms behind this young orogenic process remain to be answered. For example, processes such as the accommodation of large-scale

convergence since the start of collision and the creation of the widespread, low relief of the interior region of the Tibetan Plateau still need to be elucidated.

MT has played a major role in the tectonic studies of the Tibetan Plateau in the past few decades and can help to answer these types of questions. Many of these studies were conducted as part of the INDEPTH project (International Deep Profiling of Tibet and the Himalaya) that has undertaken a series of integrated geological and geophysical studies across the Tibetan Plateau since 1993 (Chen et al. 1996; Nelson et al. 1996; Solon et al. 2005; Unsworth et al. 2004, 2005; Wei et al. 2001, 2010). One key outcome of the MT studies is the observation of a low-resistivity crustal layer along the southern and eastern margins of the Tibetan Plateau, where the resistivity values are consistent with crustal viscosities low enough to permit crustal flow (Bai et al. 2010; Rippe and Unsworth 2010). A comprehensive review of these earlier efforts to resolve the lithospheric electrical structure of this continent–continent collision system was given by Unsworth (2010). Many MT studies have been conducted in recent years to continue investigating this complex orogenic system in the regions of the Garhwal Himalaya (Rawat et al. 2014), the Sikkim Himalaya (Pavan Kumar et al. 2014), southern Tibet (Wang et al. 2017; Xie et al. 2016), southeastern Tibet (Dong et al. 2016; Lin et al. 2017), central Tibet (Vozar et al. 2014; Zeng et al. 2015), and northern Tibet (Le Pape et al. 2015; Le Pape et al. 2012; Wei et al. 2014), as well as the eastern margin (Cai et al. 2017; Wang et al. 2014; Zhan et al. 2013; Zhang et al. 2012; Zhao et al. 2012), northeastern margin (Jin et al. 2012; Xiao et al. 2012, 2013, 2015a, 2016), and northern margin (Xiao et al. 2011, 2017; Zhang et al. 2015b, c) of the Tibetan Plateau. These studies have further revealed the complex distribution of the crustal flow beneath the Tibetan Plateau. However, to fully understand the nature of the crustal flow, a regional 3-D model is required for interpretation of the crustal flow below the Tibetan Plateau and its surrounding regions.

Under the SinoProbe Project, a 3-D MT array was deployed on the Tibetan Plateau from 2010 to 2013 to better understand the regional orogeny. By the end of 2013, 1099 MT stations were deployed, including 102 combined BBMT and LMT stations. MT data from these stations are generally of high quality, given the low level of cultural noise within most regions of the Tibetan Plateau. MT data from these 102 combined BBMT and LMT stations have been used to investigate the deep lithospheric electrical structure of the Tibetan Plateau. The station locations are shown in Fig. 24, and sites that include LMT are indicated by red symbols. For these 102 sites, the MT impedances within the period range of 10–50000 s were extracted for use in the 3-D inversions. This MT dataset was inverted with the ModEM (Egbert and Kelbert 2012; Kelbert et al. 2014) code using the standard NLCG algorithm.

The prior (and starting) model for the 3-D inversion is a uniform 100 Ωm half space. The mesh size is 39 by 66 by 45 nodes in the NS, EW, and vertical directions, respectively, with a 40 by 40 km grid in the core region. Sixteen frequencies were extracted for each station with $\sim$4 frequencies per decade. Full impedance tensors were inverted, and the error floors for all components were set to $0.05\times$ $(\mathrm{Zxy} \times \mathrm{Zyx})^{1/2}$. The initial damping parameter was set to $\lambda = 1000$ and was updated during the inversion process by dividing it by 10 each time the convergence stalled. The misfit tolerance for the forward solver was 10^{-7}. Smoothing factors in all three directions (X, Y, and Z) were 0.3. By using the inversion parameters described above, the inversion converged after 162 iterations with a final overall root-mean-square (RMS) misfit of 1.882, indicating a relatively good data fit.

Horizontal and vertical slices were extracted from this preliminary 3-D inversion model (see Figs. 25, 26, 27). It can be seen that the lithospheric electrical structure of the Tibetan Plateau shows a distinct pattern of strong variation not only vertically but also horizontally.

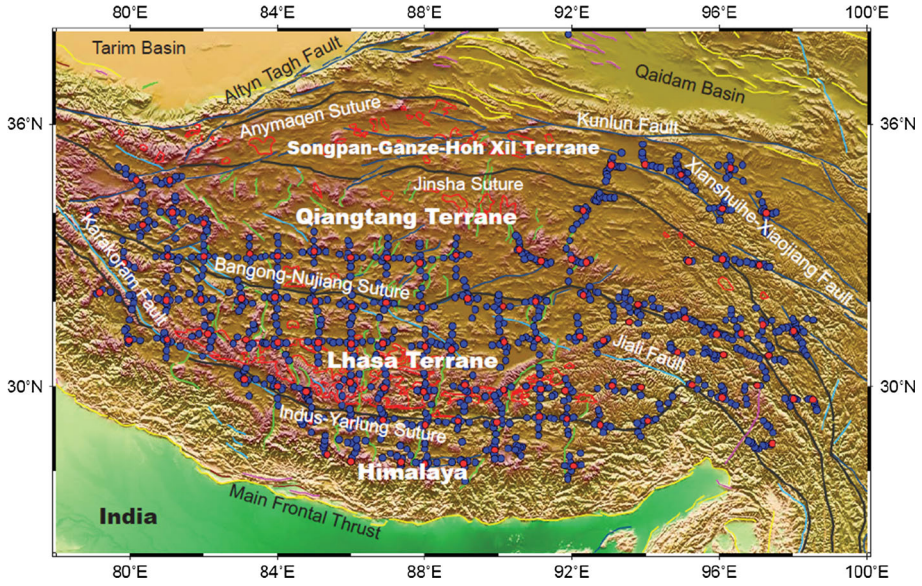

Fig. 24 Topography map showing the major tectonic structures and MT station locations in the Tibetan Plateau. Blue dots are the BBMT stations, and the red dots are the combined MT stations used in this study. Gray lines: sutures; yellow lines: thrusts; green lines: normal faults; dark blue lines: left-lateral strike-slip faults; light blue lines: right-lateral strike-slip faults; red lines: Cenozoic volcanic rocks

Conductors are pervasive in the middle-to-lower crust (see Fig. 25b). However, their geometries are complex, and not obviously consistent with the hypothesis of simple continuous eastward layer/channel flow. Instead, most crustal conductors in central and southern Tibet display a pattern of N–S extension. This feature is further confirmed from a 3-D resistivity model inverted with a subset of the SinoProbe data from Tibet, with a focus on the region of southeastern Tibetan Plateau (Dong et al. 2016).

In the depth range corresponding to the upper mantle, two more conductive regions were identified in the southern Qiangtang terrane (crossed by vertical slices a and e) and in the central Lhasa terrane (crossed by vertical slices b and g), as shown in Fig. 25c–e. These two large-scale upper mantle conductors are likely connected at even greater depths (below $\sim$300 km; see Fig. 25f).

Resistor associated with the underthrusting Indian plate can be traced beneath the Bangong–Nujiang suture in western Tibet (see Fig. 27e), but only beneath the central Lhasa terrane in central Tibet (see Fig. 27g), which might be associated with tearing of the underthrusting Indian slab, where the resistor is separated by several conductive windows that represent the upwelling of the asthenosphere through the tearing gaps (see Fig. 26c). This interpretation is supported by a recent MT study that focused on the Yadong–Gulu Rift in southern Tibet, in which a large-scale conductor in the upper mantle directly beneath the rift system was interpreted to have been caused by the tearing of the subducted Indian lithospheric slab (Wang et al. 2017). The proposed location of the tearing window is also consistent with the 3-D model presented in this paper.

Lastly, a vertical slice from a location near the previous INDEPTH 100 line is compared with the previous 2-D inversion results of Unsworth et al. (2005) in Fig. 28. Although these two models are obtained through different datasets and inverted with different approaches,

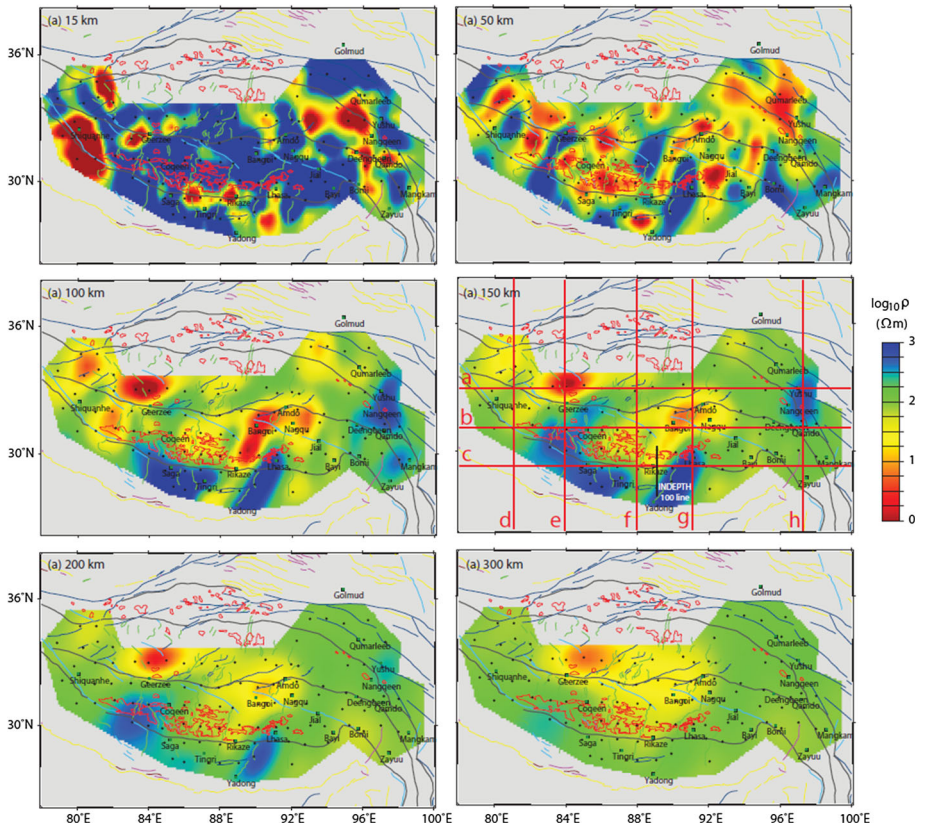

Fig. 25 Horizontal slices extracted from the 3-D inversion model of the Tibetan Plateau. Black dots are the MT station locations. Tectonic structures are the same as in Fig. 24

the results are generally consistent. Future studies will include more of the BBMT data in 3-D inversions to explore the crustal electrical structure in greater detail. For this purpose, the preliminary lithospheric model presented in this paper can be used as a starting model, after interpolation to a grid with a higher resolution.

3.2.6 The Qinling–Dabie Orogen

At the far east of the Tethyan orogenic system, the Qinling–Dabie Orogen formed as the Paleo-Tethys Ocean closed and marks the boundary between North China and South China. The Dabie Orogen is well known for its exposure of high- and ultrahigh-pressure metamorphic rocks. It has been proposed that the Dabie Orogen formed by continent–continent collision between the Yangtze and North China blocks during the Middle to Late Triassic and collapsed during the middle of the Early Cretaceous. Through 3-D inversion of the MT profile data across major collapsed structures in the Dabie Orogen (see Fig. 29), Xu et al. (2016b) established the post-collision lithospheric structure and identified domains of rejuvenated and depleted lithospheric mantle. The correlation between the extensive surface magmatism during the Early Cretaceous and a deep rejuvenated lithospheric mantle is illuminated by the elevated electrical conductivity in this area. The

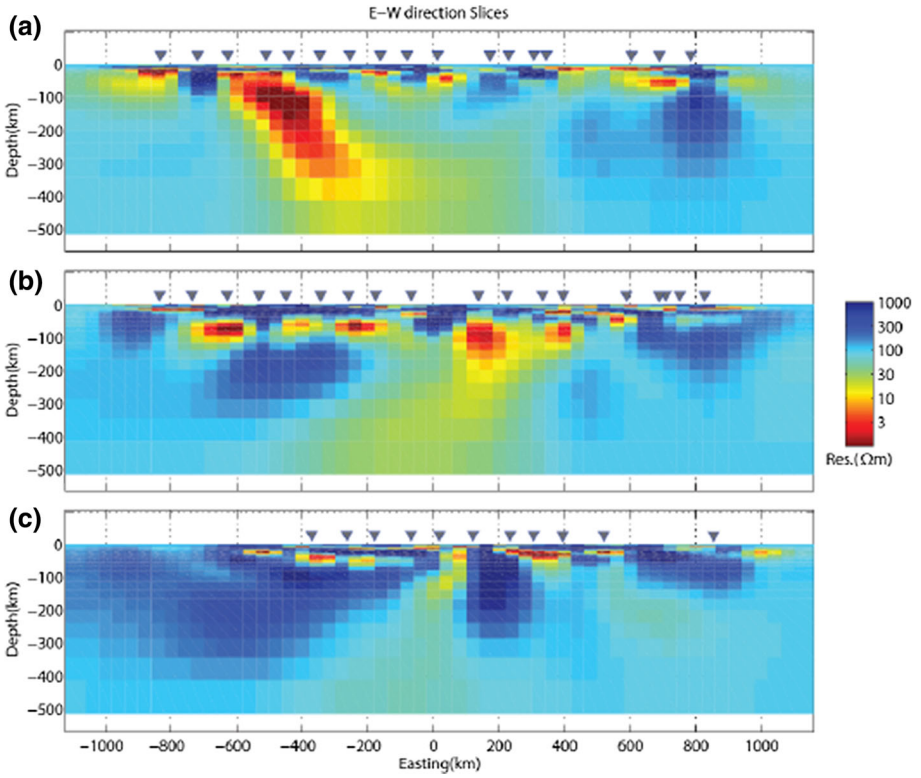

Fig. 26 E–W-directed vertical slices extracted from the 3-D inversion model of the Tibetan Plateau. Slice locations are marked in Fig. 25d

electrical model suggests that the lowermost crust beneath the eastern Dabie Orogen was removed by delamination during the orogenic collapse, whereas the residual cratonic crust is underlain by depleted lithospheric mantle with relatively high resistivity.

3.3 Comparison and Summary for Major Orogenic Systems

It can be seen that the lithospheric electrical structures of the CAOB are quite different in its western and eastern segments (see Table 1). In the western segment, the lithospheric electrical structure is characterized by a reduced resistivity with increasing depth, from the upper crust to the upper mantle (from thousands to tens of Ωm), which reflects the nature of a fossil intra-oceanic subduction zone. In the eastern segment, the lithospheric electrical structure is similar to those of the major continental blocks, with a resistive upper crust and upper mantle (hundreds to thousands of Ωm) and a relatively conductive mid-lower crust (tens to hundreds of Ωm); these observations suggest that the interior structure of this orogen was not fully destroyed during the soft collision between the continental blocks, which is consistent with the accretionary nature of the CAOB. Another intriguing feature of the CAOB is that, although some localized crustal conductors are observed, the lithospheric electrical structure of the CAOB is generally more resistive than that in the bordering continental blocks (e.g., Junggar Basin, northeastern North China Craton, and Songliao Basin, see Figs. 14, 15, 16).

In the Tethyan orogenic system, the most distinct features are the widespread conductive layers in the lower crust and upper mantle (as low as a few to several tens of Ωm, see Table 1), which make the orogenic belt more conductive than its bordering continental blocks (e.g., Arabia and India). Such a low resistivity is generally attributed to distributed aqueous fluids and/or partial melts generated during a collisional orogeny. The presence of fluids may sufficiently weaken the crust and mantle to allow lateral flow in layers or channels and may also allow decoupling of the upper and lower portions of the lithosphere. The complex distribution of crustal conductors in the Tibetan Plateau suggests that the geometry of the lateral flow is three-dimensional in nature and cannot be described by a few simple channels (see Fig. 25). The electrical features mentioned above can be seen at almost every segment along the Tethyan orogen, from its western extent to its eastern extent (e.g., Anatolian Block, Pamir, Tibetan Plateau, and Dabie Orogen), with the only exception in the transition area from the Arabia–Asia collision to the India–Asia collision (e.g., Zagros collision belt and Oman ophiolite suite). The lithospheric electrical structure of this transition area is characterized by a relatively high resistivity (see Table 1), which is similar to the electrical structure of a soft collision zone. The Arabia–Asia collision and India–Asia collision systems on either side of the transition area have similar geometries, plate motion directions, distributions of conjugate strike-slip faults, as well as lithospheric electrical structures, although the India–Asia collision system is much larger in scale.

The Central Asian orogenic system and the Tethyan orogenic system represent two distinct types of orogeny. The CAOB is a typical accretionary orogeny, which involves collision and suturing of partially juvenile crustal blocks as well as reworked older crust to continental crust along with continuing oceanic plate subduction. The Tethyan orogenic system is a typical collisional orogeny, in which the crust is considerably thickened, and thrusting, metamorphism, and partial melting rework the continental blocks and lead to the formation of juvenile crust. The distinct lithospheric electrical structures of these two orogenic systems reflect their different evolutions. In general, the lithospheric electrical structure of the Tethyan orogenic system is more conductive than that of the Central Asian orogenic system.

4 Lithospheric Electrical Structure of Subduction System

The western Pacific subduction system involves a complex interaction between the oceanic Pacific Plate (PCP) and Philippine Sea Plate (PSP) and the continental Eurasian Plate (EUP). Subduction of the Pacific Plate at the eastern margin of the Asian continent has played a significant role in the tectonic activities of East Asia, as evidenced by the widespread earthquake and volcanic activity in this region. In previous studies, the MT method has been effectively used to map the subsurface electrical structures in these volcanic regions (Aizawa et al. 2004, 2014, 2016; Kanda and Ogawa 2014; Ogawa et al. 2014) and seismogenic zones (Ichihara et al. 2008, 2011, 2014, 2016; Ogawa and Honkura 2004; Uyeshima et al. 2005; Yoshimura et al. 2008, 2009). In these studies, the MT method was commonly used to identify conductors that reflect subsurface fluid distribution, which is a crucial factor that controls earthquake and volcanic activity. However, most of these studies only resolved the electrical structure at the crustal scale. Although this information is sufficient to understand the triggering mechanism of volcanoes and earthquakes, the deep lithospheric electrical structure of the complex subduction system is still unclear. In this section, I will highlight three case studies that have mapped the subsurface electrical

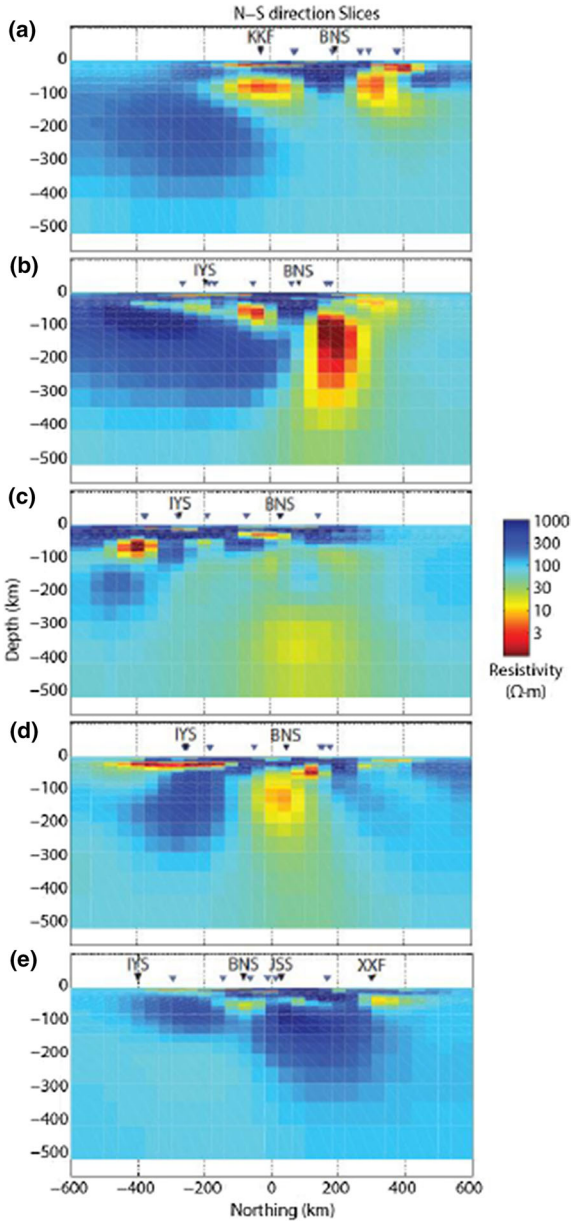

Fig. 27 N–S-directed vertical slices extracted from the 3-D inversion model of the Tibetan Plateau. Slice locations are marked in Fig. 25d. Abbreviations are as follows: *KKF* Karakoram fault, *BNS* Bangong–Nujiang Suture, *IYS* Indus–Yarlung Suture, *JSS* Jinsha suture, *XXF* Xianshuihe–Xiaojiang fault

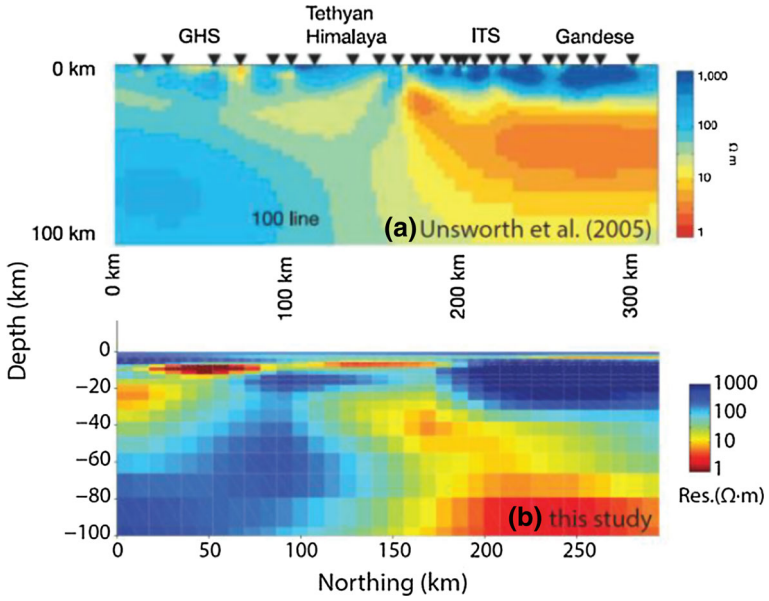

Fig. 28 Comparison of previous 2-D inversion model of INDEPTH 100 line (Unsworth et al. 2005). Vertical slice location is marked in Fig. 25d. Abbreviations are as follows: *GHS* Greater Himalayan Sequence, *ITS* Indus–Tsangpo suture

structure of this subduction system at the lithospheric scale. The study areas include, from north to south along the western Pacific subduction system, the northeast Japan subduction zone, the Kyushu subduction zone, and the Taiwan orogen.

4.1 Northeast Japan Subduction Zone

In a recent MT study conducted by Ichiki et al. (2015), a regional 3-D long-period MT array was deployed in NE Japan to investigate the lithospheric electrical structure of the subduction zone in that area. The NE Japan subduction zone was primarily formed through the subduction of the Pacific Plate along the Japan Trench. A 3-D resistivity model was obtained by incorporating information of the subducting slab from earlier studies into the inversion scheme (see Fig. 30), and a vertically continuous conductive zone has been imaged from the subducting slab surface to the lower crust, indicating a saline fluid and/or melt pathway. The observed conductivity of the lower crust corresponds to a fluid fraction of at least approximately 0.7 vol.%. Other profiles in the across-arc direction reveal that the conductive zone separates from the subducting slab surface at a depth of 80–100 km and folds back toward the back-arc, which indicates the presence of small-scale poloidal convections in the across-arc direction.

4.2 Kyushu Subduction Zone

Southwest of the NE Japan subduction zone, the Kyushu subduction zone was primarily formed through the subduction of the Philippine Sea Plate beneath the Eurasian Plate along the Nankai Trough. A 3-D lithospheric-scale electrical resistivity model beneath Kyushu Island was developed by Hata et al. (2015) using network-MT data. The network-MT

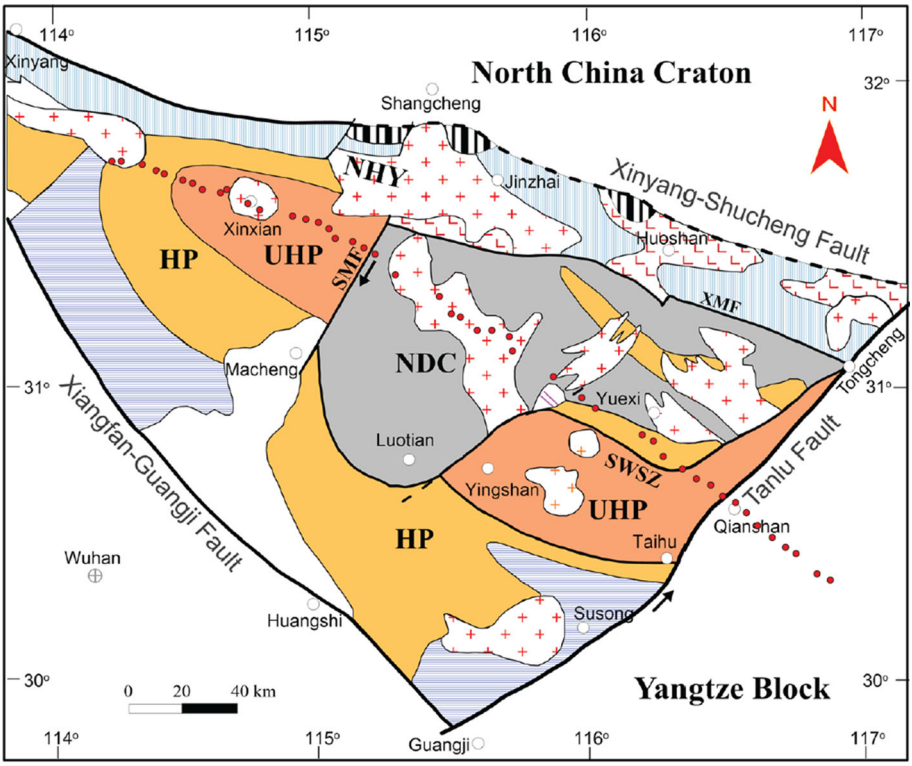
North China Craton
Yangtze Block
Xinyang
Shangcheng
Jinzhai
Huoshan
Xinyang-Shucheng Fault
NHY
HP
UHP
SMF
XMF
NDC
Macheng
Yuexi
Tongcheng
Luotian
SWSZ
Yingshan
Tanlu Fault
Taihu
Qianshan
Wuhan
Xiangfan-Guangji Fault
Huangshi
Susong
Guangji
N
114°
115°
116°
117°
32°
31°
30°
0 20 40 km
Meishan Coal Series
Metaflysch
Northern Dabie Complex (NDC)
Mesozoic Granitoid
Fault / Boundary
UHP Eclogite Unit
HP Eclogite Unit
Susong-Hong'an Group
Mesozoic Volcanics
Rapakivi
City / Town
NHY North Huaiyang Unit
XMF Xiaotian-Mozitan Fault
SMF Shangcheng-Macheng Fault
SWSZ Shuihou-Wuhe Shear Zone

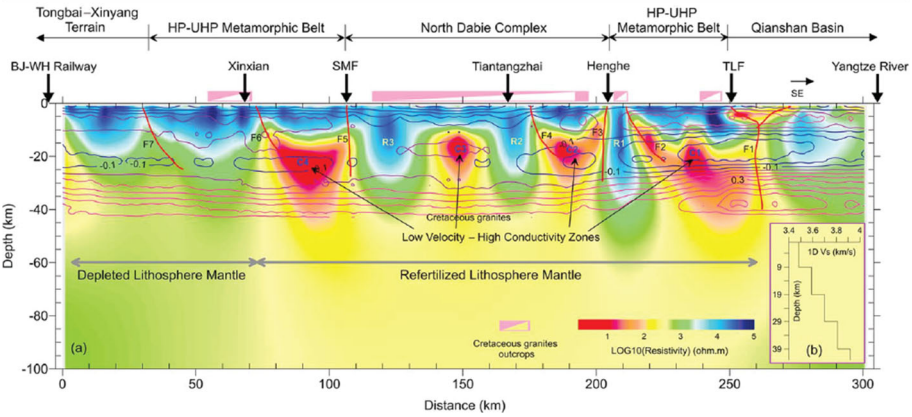
Tongbai–Xinyang Terrain
HP-UHP Metamorphic Belt
North Dabie Complex
HP-UHP Metamorphic Belt
Qianshan Basin
BJ-WH Railway
Xinxian
SMF
Tiantangzhai
Henghe
TLF
Yangtze River
SE
Depth (km)
Distance (km)
Cretaceous granites
Low Velocity – High Conductivity Zones
Depleted Lithosphere Mantle
Refertilized Lithosphere Mantle
Cretaceous granites outcrops
LOG10(Resistivity) (ohm.m)
1D Vs (km/s)
(a)
(b)

◀**Fig. 29** Simplified tectonic map of the Dabie Orogen with the location of the MT profile (upper panel) and a vertical slice extracted from the 3-D inversion model showing the electrical structure beneath the MT profile (lower panel) (modified after Xu et al. 2016b). Contour lines in subfigure (a) show the relative variations of the shear wave velocity from the baseline model in subfigure (b)

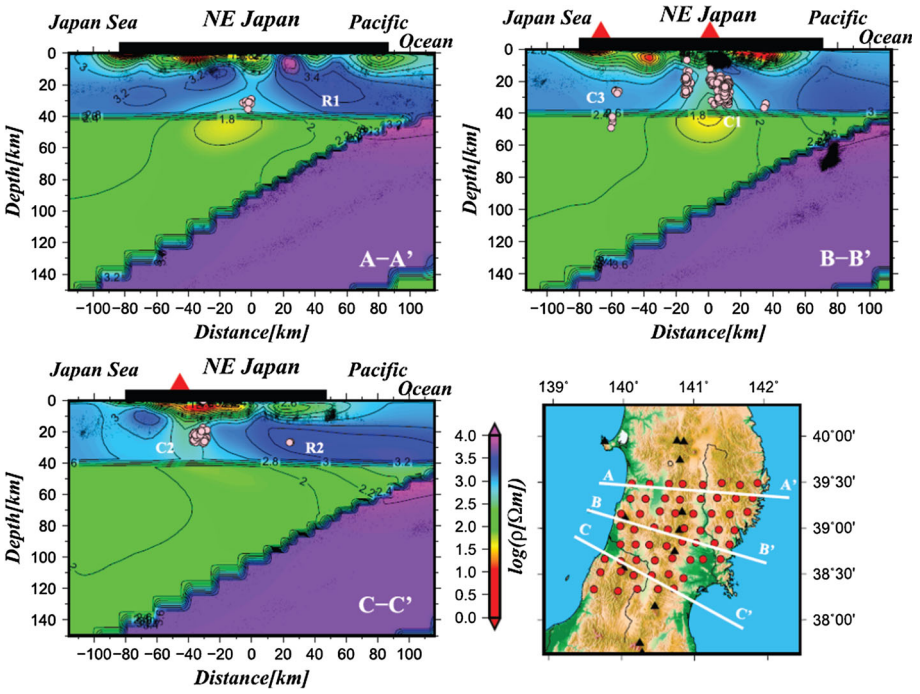

Fig. 30 Vertical profiles of the resistivity distribution perpendicular to the Japan Trench axis (from Ichiki et al. 2015)

method uses a telephone line network or purpose-built, long baseline cables to measure the voltage differences across long electrode distances to alleviate the static shift caused by small-scale, near-surface lateral heterogeneities (Uyeshima 2007). Their 3-D electrical resistivity model shows three different conductive anomalies that indicate either slab-derived aqueous fluid and/or partial melt beneath the volcanic and non-volcanic regions (see Fig. 31). The conductive anomaly beneath the northern volcanic region is far from the subducting Philippine Sea Plate and extends from the surface to less than 100 km, whereas the conductive anomaly in the southern volcanic region is next to the Philippine Sea Plate at >70 km depth, extending from the surface to over 100 km. The relatively conductive anomaly beneath the non-volcanic region is also next to the Philippine Sea Plate but only extends upward to a depth of ~50 km. The degrees of magmatism and the relative contribution of the slab-derived fluids to the magmatism vary spatially across the study region.

Based on the 3-D model, Hata and Uyeshima (2015) further proposed a new method for estimating the temperatures and melt fractions of the upper mantle by incorporating the electrical conductivity structure with the laboratory-determined relationships between the electrical conductivity and temperature of four nominally anhydrous minerals (olivine,

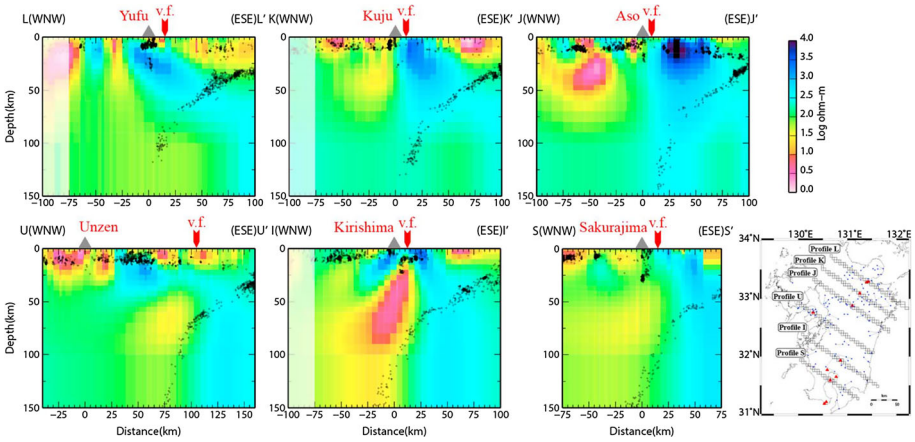

Fig. 31 Cross sections of the 3-D resistivity model of the Kyushu subduction zone along six profiles shown on the map in the bottom right-hand corner. The abbreviation v.f. is volcanic front (from Hata et al. 2015)

orthopyroxene, clinopyroxene, and garnet) and basaltic melt. The temperatures are expressed as the upper limit temperatures using the Hashin–Shtrikman lower bound for solid phases and upper bound for solid–liquid mixed phases. By assuming isobaric hydrous melting and a uniform water content of 0 wt% (dry mantle), 0.01 and 0.1 wt% (wet mantle) in the mantle wedge, the temperatures of the upper mantle are estimated to be 1100–1450 °C for the dry mantle case and 900–1350 °C for the wet mantle case, and the melt fractions of the upper mantle are <20% beneath the two volcanic regions and <5% beneath the non-volcanic region, for both dry and wet mantle cases (see Fig. 32).

4.3 Taiwan Orogen

Far to the south of the Kyushu Subduction Zone, Taiwan Island is located at the boundary between the Philippine Sea Plate and the Eurasian Plate. This plate boundary is rather complex because it comprises two subduction zones of reverse polarities. The Taiwan orogen is the result of the collision between the Luzon arc on the Philippine Sea Plate and the Eurasian continental margin, and this area is a typical example of arc–continent collision. Two different types of tectonic models have been proposed for this orogen, namely the thin-skinned and thick-skinned lithospheric deformation models, which predict contrasting mid-lower crust structures.

In the studies of Bertrand et al. (2009, 2012), three long-period MT transects across south, central, and north Taiwan were completed and modeled with 2-D inversion (see Fig. 33). The MT models beneath south and central Taiwan imaged a prominent conductor extending across the hypothetical décollement predicted by the thin-skinned model. By contrast, the thick-skinned model predicts this conductive feature, as fluids are generated in the crustal root through metamorphism. Quantitative correlation of the electrical resistivity and seismic velocity models supports the interpretation that the conductive feature represents a small volume of high-salinity fluids in a thickened crust. The resistivity model for northern Taiwan is consistent with dehydration of the subducting Philippine Sea Plate and with deformation described by the subducting-induced tectonic model, suggesting that the Eurasian plate is absent and likely removed by slab break-off beneath northern Taiwan. Modeling of the full dataset has shown that electrically conductive, seismically active

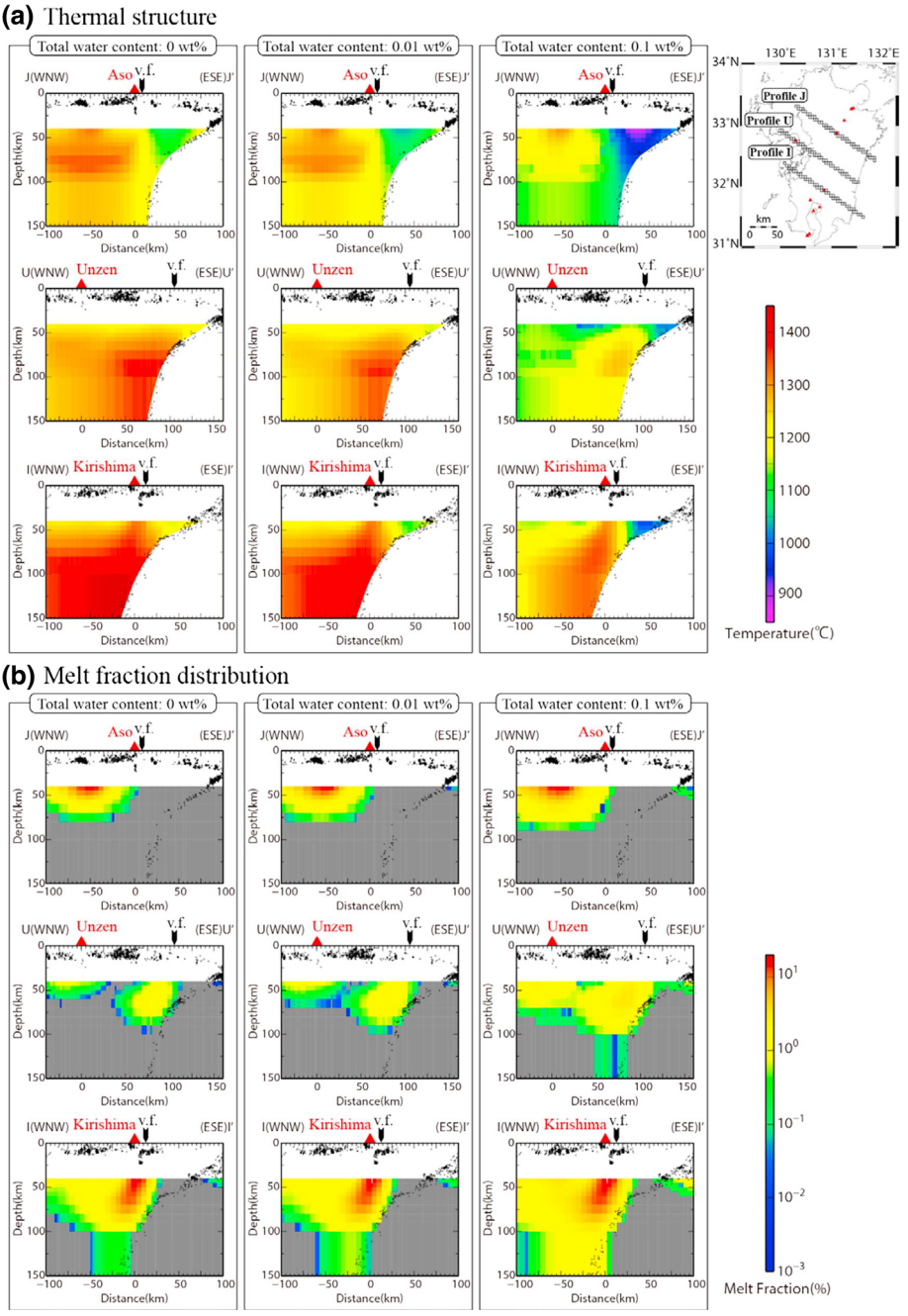

Fig. 32 **a** Cross sections of the thermal structure of the mantle wedge beneath the Kyushu subduction zone along the three profiles shown on the map in the upper right-hand corner. **b** Cross sections of the melt fraction distributions. The abbreviation v.f. is volcanic front (from Hata and Uyeshima 2015)

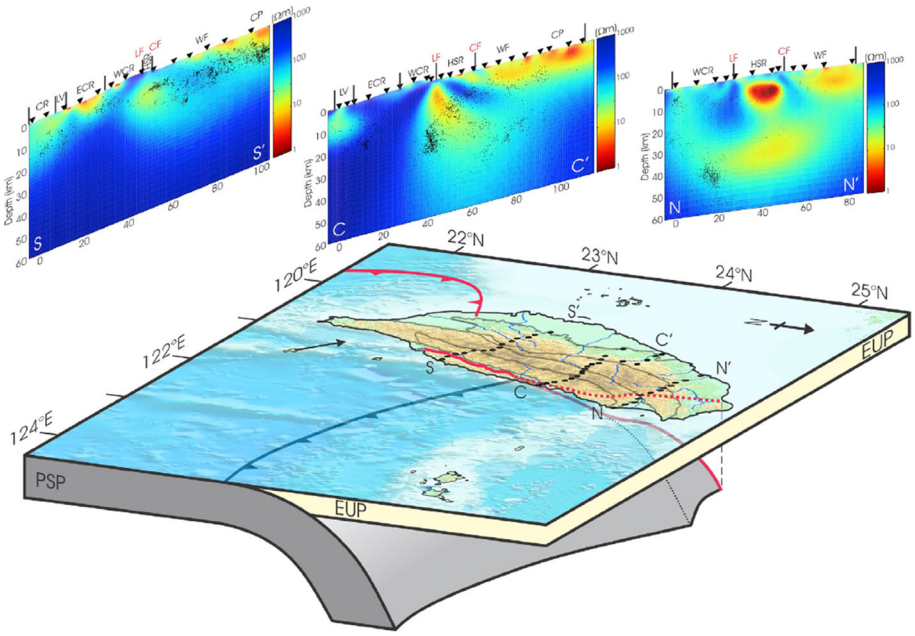

Fig. 33 Schematic of the plate convergence in the region of the Taiwan orogen, shown with the 2-D inversion models of three MT profiles (from Bertrand et al. 2012). Abbreviations are as follows: *CP* coastal plain, *WF* western foothills, *HSR* Hsuehshan Range, *W/ECR* western/eastern Central Range, *LV* longitudinal valley, *CR* coastal range, *CF* Chuchih fault, *LF* Lishan fault, *EUP* Eurasian Plate, *PSP* Philippine Sea Plate

crustal structures exist at depths greater than 30 km beneath the Taiwan orogen. These conductive regions, interpreted as interconnected fluid pathways, map pervasive zones of collisional deformation at a lithospheric scale.

4.4 Comparison and Summary for the Western Pacific Subduction System

In summary, according to the three case studies discussed earlier in this section, the lithospheric electrical structure of the western Pacific subduction system comprises the resistive subducting Pacific and Philippine Sea Plates (several thousands of Ωm) and conductive upper crust and mantle wedge of the Eurasian Plate (a few to hundreds of Ωm, see Table 1). The Pacific plate is several times more resistive than the Philippine Sea Plate. The electrical structures of the mid-lower crust above the subducting slabs differ between study regions. In the NE Japan subduction zone, the mid-lower crust is generally resistive ($\sim$1000 Ωm). By contrast, the mid-lower crust beneath the Kyushu subduction zone consists of a resistive fore-arc (>1000 Ωm) and a conductive back-arc ($\sim$10 Ωm). In contrast to the layered distribution of crustal conductors in the Tethyan orogenic system, subvertical conductors are commonly seen rising from above the subducting slab surface to the upper crust beneath the volcanic arcs, indicating the pathways of saline fluids and/or partial melts (see Figs. 30, 31).

Another intriguing feature of the western Pacific subduction system is the increasing complexity and variation in the lithospheric electrical structures from the northern extent to the southern extent of this system. In the northern part of the NE Japan subduction zone, minor latitudinal changes are observed and a vertically continuous conductive zone is

imaged from the subducting slab surface to the lower crust, indicating a saline fluid and/or melt pathway (see Fig. 30). However, in the Kyushu subduction zone, conductive anomalies vary spatially beneath the volcanic and non-volcanic regions, within tens of kilometers in the N–S direction (see Fig. 31), suggesting that the geometry of the subducting Philippine Sea Plate is much more complex than that of the Pacific Plate. In the Taiwan orogen, the spatial variation in the N–S direction is even stronger. In southern and central Taiwan, the lithosphere consists of a conductive Eurasian Plate and resistive Philippine Sea Plate with deeply extended conductors that indicate fluids generated in the thickened crust through metamorphism (see profiles S–S′ and C–C′ in Fig. 33). However, in northern Taiwan, the lithospheric electrical structure is characterized by pervasive conductors in the crust and upper mantle, suggesting that the Eurasian Plate is absent beneath northern Taiwan due to slab break-off (see profile N–N′ in Fig. 33).

5 Conclusions

Asia is the largest and youngest continent on Earth and was formed through the amalgamation of several major continental blocks formerly separated by the Paleo-Asian and Tethyan Oceans. During this process, the Asian continent underwent a long period of continental crustal growth and tectonic deformation. To understand the complex evolution and deformation mechanisms of the Asian continent, geophysical electromagnetic methods, mainly the magnetotelluric (MT) method, have been widely used in recent decades to image the subsurface electrical structures. In this review, case studies were summarized to highlight the recent developments in the study of the regional lithospheric electrical structures under diverse tectonic settings across the Asian continent. These case studies focused on the major continental blocks of Asia, the Central Asian orogenic system, the Tethyan orogenic system, and the western Pacific subduction system.

In conclusion, most major continental blocks of Asia exhibit a three-layer structure of resistive upper crust, relatively conductive mid-lower crust and resistive upper mantle. The distribution of the mid-lower crustal conductors is generally localized in the stable continental blocks, with locations strongly correlated with the paleo-sutures or fossil subduction zones. Large-scale conductors in the upper mantle were also observed, indicating the modification of the marginal cratonic lithosphere. The Central Asian orogenic system and the Tethyan orogenic system represent two distinct types of orogeny. The lithospheric electrical structure of the accretionary Central Asian orogenic system is different in its western and eastern segments and is generally more resistive than the bordering continental blocks. While the collisional Tethyan orogenic system is more conductive, with widespread conductive layers in the lower crust and upper mantle, which are attributed to aqueous fluids and/or partial melts that may sufficiently weaken the lithosphere to allow lateral flow. The western Pacific subduction system comprises the resistive subducting Pacific and Philippine Sea Plates and conductive Eurasian Plate, with increasing complexity and variation in the lithospheric electrical structures from north to south. In general, the following areas of the Asian continent have increasingly conductive lithospheric electrical structures, which correspond to the transition from the most stable to the most active tectonic areas of the Asian continent: the major continental blocks, the accretionary Central Asian orogenic system, the collisional Tethyan orogenic system, and the western Pacific subduction system.

As a key part of this review, a 3-D model of the lithospheric electrical structure of a large portion of the Tibetan Plateau was presented and discussed in detail. The preliminary 3-D inversion model showed a strong variation in the electrical structures not only vertically but also horizontally. The complex geometries of the conductors are not obviously consistent with the hypothesis of continuous eastward channel flow and instead suggest extension in the N–S direction. In the upper mantle, the southern Qiangtang and central Lhasa terranes are two of the most conductive regions. The underthrust resistive Indian plate can be traced beneath the Bangong–Nujiang suture in western Tibet, but beneath only the central Lhasa terrane in central Tibet, which may be associated with tearing of the underthrusting Indian slab.

The case studies discussed in this review not only prove the effectiveness of the MT method but also considerably enhance our knowledge of the formation mechanisms of the Asian continent. However, to achieve a comprehensive understanding of this process, further studies are still needed. Here I suggest future research in the following three aspects. First, field data are needed from regions not covered by previous studies (e.g., the Siberia and Tarim Cratons, vast areas of the CAOB and Southeast Asia) to obtain complete data coverage at the continental scale. Second, although significant progress has been made in recent years, improvements on data processing, analysis, and inversion techniques are needed in the near future to address the large-scale 3-D array data. Such improvements are important not only for obtaining high-quality data from the increasingly noisy environment but also for reliably resolving the 3-D lithospheric electrical structure at the continental scale. Third, integration of the EM data with other geophysical or geological data is strongly suggested. This integration should include research on the subjects of joint/constrained inversion of EM data with other geophysical data (Moorkamp 2017), as well as quantitative interpretation by correlating the electrical resistivity with other physical properties of the lithosphere (e.g., temperature, viscosity, water content, and melt fraction). Future integration efforts should also include the discipline of space science, in which the lithospheric electrical model can be used as an input to predict magnetic storm hazards for power grids (Love et al. 2017).

Acknowledgements I am grateful to Prof. Ian Ferguson and the program committee of 23rd EMIW for their kind invitation to present this review. The author would also like to thank Prof. Wenbo Wei, Prof. Sheng Jin, Prof. Gaofeng Ye and other colleagues from the CUGB MT group for their support in finishing this review. Dr. Abdul Azeez, Prof. Alan Jones, Prof. Behrooz Oskooi, Prof. Gary Egbert, Dr. Makoto Uyeshima, Prof. Martyn Unsworth, Prof. Oliver Ritter, Dr. Prasanta Patro, Dr. Stephan Thiel, Dr. Ted Bertrand, Prof. Vladimir Semenov, Prof. Yasuo Ogawa, as well as many other colleagues whose work have been cited in this review, are highly appreciated for their contribution to this paper. Sincere thanks to Dr. Kiyoshi Baba and the other two anonymous reviewers, whose detailed comments and constructive suggestions helped to make the manuscript more comprehensive and solid. This work was jointly supported by Project SinoProbe (SinoProbe-01, SinoProbe-02-04), National Natural Science Foundation of China (41774087, 41404060, 41404059), Fundamental Research Funds for the Central Universities (2652017417), and Open Fund of Key Laboratory of Geo-detection (China University of Geosciences, Beijing), Ministry of Education (GDL1501).

References

Abdul Azeez KK (2016) Magnetotelluric constraints on the occurrence of lower crustal earthquakes in the intra-plate setting of central Indian tectonic zone. Acta Geologica Sinica–English Edition 90(3):884–899. doi:10.1111/1755-6724.12731

Abdul Azeez KK, Unsworth MJ, Patro PK, Harinarayana T, Sastry RS (2013) Resistivity structure of the Central Indian Tectonic Zone (CITZ) from multiple magnetotelluric (MT) profiles and tectonic implications. Pure Appl Geophys 170(12):2231–2256. doi:10.1007/s00024-013-0649-y

Abdul Azeez KK, Veeraswamy K, Gupta AK, Babu N, Chandrapuri S, Harinarayana T (2015) The electrical resistivity structure of lithosphere across the Dharwar craton nucleus and Coorg block of South Indian shield: evidence of collision and modified and preserved lithosphere. J Geophys Res Solid Earth 120(10):6698–6721. doi:10.1002/2014JB011854

Abdul Azeez KK, Patro PK, Harinarayana T, Sarma SVS (2017) Magnetotelluric imaging across the tectonic structures in the eastern segment of the Central Indian Tectonic Zone: preserved imprints of polyphase tectonics and evidence for suture status of the Tan Shear. Precambr Res 298:325–340. doi:10.1016/j.precamres.2017.06.018

Aizawa K, Yoshimura R, Oshiman N (2004) Splitting of the Philippine Sea Plate and a magma chamber beneath Mt. Fuji. Geophys Res Lett 31(9):L09603. doi:10.1029/2004GL019477

Aizawa K, Koyama T, Hase H, Uyeshima M, Kanda W, Utsugi M, Yoshimura R, Yamaya Y, Hashimoto T, Ki Yamazaki, Komatsu S, Watanabe A, Miyakawa K, Ogawa Y (2014) Three-dimensional resistivity structure and magma plumbing system of the Kirishima Volcanoes as inferred from broadband magnetotelluric data. J Geophys Res: Solid Earth 119(1):198–215. doi:10.1002/2013JB010682

Aizawa K, Sumino H, Uyeshima M, Yamaya Y, Hase H, Takahashi HA, Takahashi M, Kazahaya K, Ohno M, Rung-Arunwan T, Ogawa Y (2016) Gas pathways and remotely triggered earthquakes beneath Mount Fuji Japan. Geology 44(2):127–130. doi:10.1130/g37313.1

Avşar Ü, Türkoğlu E, Unsworth M, Çağlar İ, Kaypak B (2013) Geophysical images of the North Anatolian Fault Zone in the Erzincan Basin, Eastern Turkey, and their tectonic implications. Pure Appl Geophys 170(3):409–431. doi:10.1007/s00024-012-0521-5

Bai D, Unsworth MJ, Meju MA, Ma X, Teng J, Kong X, Sun Y, Sun J, Wang L, Jiang C, Zhao C, Xiao P, Liu M (2010) Crustal deformation of the eastern Tibetan plateau revealed by magnetotelluric imaging. Nature Geosci 3(5):358–362 http://www.nature.com/ngeo/journal/v3/n5/suppinfo/ngeo830_S1.html

Bertrand E, Unsworth M, Chiang C-W, Chen C-S, Chen C-C, Wu F, Türkoğlu E, Hsu H-L, Hill G (2009) Magnetotelluric evidence for thick-skinned tectonics in central Taiwan. Geology 37(8):711–714. doi:10.1130/g25755a.1

Bertrand EA, Unsworth MJ, Chiang C-W, Chen C-S, Chen C-C, Wu FT, Türkoğlu E, Hsu H-L, Hill GJ (2012) Magnetotelluric imaging beneath the Taiwan orogen: an arc-continent collision. Solid Earth, J Geophys Res. doi:10.1029/2011JB008688

Boonchaisuk S, Siripunvaraporn W, Ogawa Y (2013) Evidence for middle Triassic to Miocene dual subduction zones beneath the Shan-Thai terrane, western Thailand from magnetotelluric data. Gondwana Res 23(4):1607–1616. doi:10.1016/j.gr.2012.08.009

Cai J, Chen X, Xu X, Tang J, Wang L, Guo C, Han B, Dong Z (2017) Rupture mechanism and seismotectonics of the Ms6.5 Ludian earthquake inferred from three-dimensional magnetotelluric imaging. Geophys Res Lett 44(3):1275–1285. doi:10.1002/2016GL071855

Chave AD, Jones AG (2012) The magnetotelluric method: theory and practice. Cambridge University Press, Cambridge

Chen L, Booker JR, Jones AG, Wu N, Unsworth MJ, Wei W, Tan H (1996) Electrically conductive crust in Southern Tibet from INDEPTH Magnetotelluric Surveying. Science 274(5293):1694–1696. doi:10.1126/science.274.5293.1694

Dong S, Li T, Gao R, Hou H, Li Q, Li Y, Zhang S, Keller GR, Liu M (2011) A multidisciplinary Earth science research program in China. EOS Trans AGU 92(38):313–314

Dong S-W, Li T-D, Lü Q-T, Gao R, Yang J-S, Chen X-H, Wei W-B, Zhou Q (2013) Progress in deep lithospheric exploration of the continental China: a review of the SinoProbe. Tectonophysics 606:1–13. doi:10.1016/j.tecto.2013.05.038

Dong H, Wei W, Ye G, Jin S, Jones AG, Jing J, Zhang L, Xie C, Zhang F, Wang H (2014) Three-dimensional electrical structure of the crust and upper mantle in Ordos Block and adjacent area: evidence of regional lithospheric modification. Geochem Geophys Geosyst 15(6):2414–2425. doi:10.1002/2014GC005270

Dong Z, Tang J, Unsworth M, Chen X (2015) Electrical resistivity structure of the upper mantle beneath Northeastern China: implications for rheology and the mechanism of craton destruction. J Asian Earth Sci 100:115–131. doi:10.1016/j.jseaes.2015.01.008

Dong H, Wei W, Jin S, Ye G, Zhang L, Je Jing, Yin Y, Xie C, Jones AG (2016) Extensional extrusion: insights into south-eastward expansion of Tibetan Plateau from magnetotelluric array data. Earth Planet Sci Lett 454:78–85. doi:10.1016/j.epsl.2016.07.043

Egbert GD, Kelbert A (2012) Computational recipes for electromagnetic inverse problems. Geophys J Int 189(1):251–267. doi:10.1111/j.1365-246X.2011.05347.x

Gokarn SG, Gupta G, Rao CK (2004) Geoelectric structure of the Dharwar Craton from magnetotelluric studies: archean suture identified along the Chitradurga-Gadag schist belt. Geophys J Int 158(2):712–728. doi:10.1111/j.1365-246X.2004.02279.x

Harinarayana T (2007) Comparison of electrical structure of the deep crust of the central Indian Shear Zone, Narmada-Son Lineament, Deccan Traps, Southern Granulite region and Eastern Dharwar Craton. Gondwana Res 10:251–261

Hata M, Uyeshima M (2015) Temperature and melt fraction distributions in a mantle wedge determined from the electrical conductivity structure: application to one nonvolcanic and two volcanic regions in the Kyushu subduction zone, Japan. Geophys Res Lett. doi:10.1002/2015GL063308

Hata M, Oshiman N, Yoshimura R, Tanaka Y, Uyeshima M (2015) Three-dimensional electromagnetic imaging of upwelling fluids in the Kyushu subduction zone, Japan. J Geophys Res: Solid Earth 120(1):1–17. doi:10.1002/2014JB011336

Ichihara H, Honda R, Mogi T, Hase H, Kamiyama H, Yamaya Y, Ogawa Y (2008) Resistivity structure around the focal area of the 2004 Rumoi-Nanbu earthquake (M 6.1), Northern Hokkaido, Japan. Earth, Planets Space 60(8):883–888. doi:10.1186/bf03352841

Ichihara H, Uyeshima M, Sakanaka S, Ogawa T, Mishina M, Ogawa Y, Nishitani T, Yamaya Y, Watanabe A, Morita Y, Yoshimura R, Usui Y (2011) A fault-zone conductor beneath a compressional inversion zone, northeastern Honshu, Japan. Geophys Res Lett 38(9):L09301. doi:10.1029/2011GL047382

Ichihara H, Sy Sakanaka, Mishina M, Uyeshima M, Nishitani T, Ogawa Y, Yamaya Y, Mogi T, Amita K, Miura T (2014) A 3-D electrical resistivity model beneath the focal zone of the 2008 Iwate-Miyagi Nairiku earthquake (M 7.2). Earth Planets Space. doi:10.1186/1880-5981-66-50

Ichihara H, Mogi T, Tanimoto K, Yamaya Y, Hashimoto T, Uyeshima M, Ogawa Y (2016) Crustal structure and fluid distribution beneath the southern part of the Hidaka collision zone revealed by 3-D electrical resistivity modeling. Geochem Geophys Geosyst 17(4):1480–1491. doi:10.1002/2015GC006222

Ichiki M, Ogawa Y, Kaida T, Koyama T, Uyeshima M, Demachi T, Hirahara S, Honkura Y, Kanda W, Kono T, Matsushima M, Nakayama T, Suzuki S, Toh H (2015) Electrical image of subduction zone beneath northeastern Japan. J Geophys Res: Solid Earth 120(12):7937–7965. doi:10.1002/2015JB012028

Jin S, Zhang L-T, Jin Y-J, Wei W-B, Ye G-F (2012) Crustal electrical structure along the Hezuo-Dajing profile across the Northeastern Margin of the Tibetan Plateau. Chin J Geophys-Chin Ed 55(12):3979–3990

Jones AG (1992) Electrical conductivity of the continental lower crust. continental lower crust. Elsevier, New York, pp 81–143

Kanda W, Ogawa Y (2014) Three-dimensional electromagnetic imaging of fluids and melts beneath the NE Japan arc revisited by using geomagnetic transfer function data. Earth, Planets Space 66(1):1–8. doi:10.1186/1880-5981-66-39

Kaya T, Tank SB, Tunçer MK, Rokoityansky II, Tolak E, Savchenko T (2009) Asperity along the North Anatolian Fault imaged by magnetotellurics at Düzce, Turkey. Earth, Planets and Space 61(7):871–884. doi:10.1186/bf03353198

Kaya T, Kasaya T, Tank SB, Ogawa Y, Tunçer MK, Oshiman N, Honkura Y, Matsushima M (2013) Electrical characterization of the North Anatolian Fault Zone underneath the Marmara Sea, Turkey by ocean bottom magnetotellurics. Geophys J Int 193(2):664–677. doi:10.1093/gji/ggt025

Kelbert A, Meqbel N, Egbert GD, Tandon K (2014) ModEM: a modular system for inversion of electromagnetic geophysical data. Comput Geosci 66:40–53. doi:10.1016/j.cageo.2014.01.010

Le Pape F, Jones AG, Vozar J, Wenbo W (2012) Penetration of crustal melt beyond the Kunlun Fault into northern Tibet. Nat Geosci 5(5):330–335. doi:10.1038/ngeo1449

Le Pape F, Jones AG, Unsworth MJ, Vozar J, Wei W, Jin S, Ye G, Jing J, Dong H, Zhang L, Xie C (2015) Constraints on the evolution of crustal flow beneath Northern Tibet. Geochem Geophys Geosyst 16(12):4237–4260. doi:10.1002/2015GC005828

Liang H-D, Gao R, Hou H-S, Liu G-X, Han J-T, Han S (2015) Lithospheric electrical structure of the Great Xing'an Range. J Asian Earth Sci 113:501–507. doi:10.1016/j.jseaes.2015.01.026

Lin C, Peng M, Tan H, Xu Z, Li Z-H, Kong W, Tong T, Wang M, Zeng W (2017) Crustal structure beneath Namche Barwa, eastern Himalayan syntaxis: new insights from three-dimensional magnetotelluric imaging. J Geophys Res: Solid Earth. doi:10.1002/2016JB013825 **Inpress**

Liu L, Hasterok D (2016) High-resolution lithosphere viscosity and dynamics revealed by magnetotelluric imaging. Science 353(6307):1515–1519. doi:10.1126/science.aaf6542

Love JJ, Bedrosian PA, Schultz A (2017) Down to earth with an electric hazard from space. Space Weather 15(5):658–662. doi:10.1002/2017SW001622

Moorkamp M (2017) Integrating electromagnetic data with other geophysical observations for enhanced imaging of the earth: a tutorial and review. Surv Geophys. doi:10.1007/s10712-017-9413-7

Naganjaneyulu K, Santosh M (2012) The nature and thickness of lithosphere beneath the Archean Dharwar Craton, southern India: a magnetotelluric model. J Asian Earth Sci 49:349–361. doi:10.1016/j.jseaes.2011.07.002

Nelson KD, Zhao W, Brown LD, Kuo J, Che J, Liu X, Klemperer SL, Makovsky Y, Meissner R, Mechie J, Kind R, Wenzel F, Ni J, Nabelek J, Leshou C, Tan H, Wei W, Jones AG, Booker J, Unsworth M, Kidd WSF, Hauck M, Alsdorf D, Ross A, Cogan M, Wu C, Sandvol E, Edwards M (1996) Partially molten middle crust beneath Southern Tibet: synthesis of project INDEPTH results. Science 274(5293):1684–1688. doi:10.1126/science.274.5293.1684

Ogawa Y, Honkura Y (2004) Mid-crustal electrical conductors and their correlations to seismicity and deformation at Itoigawa-Shizuoka Tectonic Line, Central Japan. Earth, Planets Space 56(12):1285–1291. doi:10.1186/bf03353352

Ogawa Y, Ichiki M, Kanda W, Mishina M, Asamori K (2014) Three-dimensional magnetotelluric imaging of crustal fluids and seismicity around Naruko volcano, NE Japan. Earth, Planets Space 66(1):1–13. doi:10.1186/s40623-014-0158-y

Oskooi B, Pedersen LB, Koyi HA (2014) Magnetotelluric signature for the Zagros collision. Geophys J Int 196(3):1299–1310. doi:10.1093/gji/ggt466

Oskooi B, Mansoori I, Pedersen LB, Koyi HA (2015) A Magnetotelluric Survey of Ophiolites in the Neyriz area of southwestern Iran. Pure Appl Geophys 172(2):491–502. doi:10.1007/s00024-014-0925-5

Patro PK, Sarma SVS (2009) Lithospheric electrical imaging of the Deccan trap covered region of western India. J Geophys Res: Solid Earth. doi:10.1029/2007JB005572

Patro PK, Sarma SVS (2016) Evidence for an extensive intrusive component of the Deccan Large Igneous Province in the Narmada Son Lineament region, India from three dimensional magnetotelluric studies. Earth Planet Sci Lett 451:168–176. doi:10.1016/j.epsl.2016.07.005

Patro BPK, Brasse H, Sarma SVS, Harinarayana T (2005) Electrical structure of the crust below the Deccan Flood Basalts (India), inferred from magnetotelluric soundings. Geophys J Int 163(3):931–943. doi:10.1111/j.1365-246X.2005.02789.x

Patro PK, Sarma SVS, Naganjaneyulu K (2014) Three-dimensional lithospheric electrical structure of Southern Granulite Terrain, India and its tectonic implications. J Geophys Res: Solid Earth 119(1):71–82. doi:10.1002/2013JB010430

Pavan Kumar G, Manglik A, Thiagarajan S (2014) Crustal geoelectric structure of the Sikkim Himalaya and adjoining Gangetic foreland basin. Tectonophysics 637:238–250. doi:10.1016/j.tecto.2014.10.009

Petrishchev MS, Semenov VY (2013) Secular variations of the Earth's apparent resistivity. Earth Planet Sci Lett 361:1–6. doi:10.1016/j.epsl.2012.11.027

Qiu J (2013) China's exquisite look at earth's rocky husk wins raves. Science 341(6141):20

Rawat G, Arora BR, Gupta PK (2014) Electrical resistivity cross-section across the Garhwal Himalaya: proxy to fluid-seismicity linkage. Tectonophysics 637:68–79. doi:10.1016/j.tecto.2014.09.015

Rippe D, Unsworth M (2010) Quantifying crustal flow in Tibet with magnetotelluric data. Phys Earth Planet Inter 179(3–4):107–121. doi:10.1016/j.pepi.2010.01.009

Rippe D, Unsworth MJ, Currie CA (2013) Magnetotelluric constraints on the fluid content in the upper mantle beneath the southern Canadian Cordillera: implications for rheology. J Geophys Res: Solid Earth 118(10):5601–5624. doi:10.1002/jgrb.50255

Rodi W, Mackie RL (2001) Nonlinear conjugate gradients algorithm for 2-D magnetotelluric inversion. Geophysics 66(1):174–187. doi:10.1190/1.1444893

Safonova I, Maruyama S (2014) Asia: a frontier for a future supercontinent Amasia. Int Geol Rev 56(9):1051–1071. doi:10.1080/00206814.2014.915586

Sass P, Ritter O, Ratschbacher L, Tympel J, Matiukov VE, Rybin AK, Batalev VY (2014) Resistivity structure underneath the Pamir and Southern Tian Shan. Geophys J Int 198(1):564–579. doi:10.1093/gji/ggu146

Siripunvaraporn W, Egbert G (2009) WSINV3DMT: vertical magnetic field transfer function inversion and parallel implementation. Phys Earth Planet Inter 173(3–4):317–329. doi:10.1016/j.pepi.2009.01.013

Siripunvaraporn W, Egbert G, Lenbury Y, Uyeshima M (2005) Three-dimensional magnetotelluric inversion: data-space method. Phys Earth Planet Inter 150(1–3):3–14. doi:10.1016/j.pepi.2004.08.023

Solon KD, Jones AG, Nelson KD, Unsworth MJ, Kidd WF, Wei W, Tan H, Jin S, Deng M, Booker JR, Li S, Bedrosian P (2005) Structure of the crust in the vicinity of the Banggong-Nujiang suture in central Tibet from INDEPTH magnetotelluric data. J Geophys Res: Solid Earth. doi:10.1029/2003JB002405

Tank SB, Honkura Y, Ogawa Y, Oshiman N, Tunçer MK, Matsushima M, Çelik C, Tolak E, Işıkara AM (2003) Resistivity structure in the western part of the fault rupture zone associated with the 1999 İzmit earthquake and its seismogenic implication. Earth, Planets Space 55(7):437–442. doi:10.1186/bf03351777

Tank SB, Honkura Y, Ogawa Y, Matsushima M, Oshiman N, Tunçer MK, Çelik C, Tolak E, Işıkara AM (2005) Magnetotelluric imaging of the fault rupture area of the 1999 İzmit (Turkey) earthquake. Phys Earth Planet Inter 150(1–3):213–225. doi:10.1016/j.pepi.2004.08.033

Thiel S, Heinson G, Gray DR, Gregory RT (2009) Ophiolite emplacement in NE Oman: constraints from magnetotelluric sounding. Geophys J Int 176(3):753–766. doi:10.1111/j.1365-246X.2008.04053.x

Türkoğlu E, Unsworth M, Çağlar İ, Tuncer V, Avşar Ü (2008) Lithospheric structure of the Arabia-Eurasia collision zone in eastern Anatolia: magnetotelluric evidence for widespread weakening by fluids? Geology 36(8):619–622. doi:10.1130/g24683a.1

Türkoğlu E, Unsworth M, Bulut F, Çağlar İ (2015) Crustal structure of the North Anatolian and East Anatolian Fault Systems from magnetotelluric data. Phys Earth Planet Inter 241:1–14. doi:10.1016/j.pepi.2015.01.003

Unsworth M (2010) Magnetotelluric studies of active continent-continent collisions. Surv Geophys 31(2):137–161. doi:10.1007/s10712-009-9086-y

Unsworth M, Wenbo W, Jones AG, Li S, Bedrosian P, Booker J, Sheng J, Ming D, Handong T (2004) Crustal and upper mantle structure of northern Tibet imaged with magnetotelluric data. J Geophys Res: Solid Earth. doi:10.1029/2002JB002305

Unsworth M, Jones AG, Wei W, Marquis G, Gokarn SG, Spratt JE (2005) Crustal rheology of the Himalaya and Southern Tibet inferred from magnetotelluric data. Nature 438(7064):78–81. doi:10.1038/nature04154

Uyeshima M (2007) EM Monitoring of crustal processes including the use of the network-MT Observations. Surv Geophys 28(2):199–237. doi:10.1007/s10712-007-9023-x

Uyeshima M, Ogawa Y, Honkura Y, Koyama S, Ujihara N, Mogi T, Yamaya Y, Harada M, Yamaguchi S, Shiozaki I, Noguchi T, Kuwaba Y, Tanaka Y, Mochido Y, Manabe N, Nishihara M, Saka M, Serizawa M (2005) Resistivity imaging across the source region of the 2004 Mid-Niigata Prefecture earthquake (M6.8), central Japan. Earth, Planets Space 57(5):441–446. doi:10.1186/bf03351831

Vozar J, Jones AG, Fullea J, Agius MR, Lebedev S, Le Pape F, Wei W (2014) Integrated geophysical-petrological modeling of lithosphere-asthenosphere boundary in central Tibet using electromagnetic and seismic data. Geochem Geophys Geosyst 15(10):3965–3988. doi:10.1002/2014GC005365

Wang X, Zhang G, Fang H, Luo W, Zhang W, Zhong Q, Cai X, Luo H (2014) Crust and upper mantle resistivity structure at middle section of Longmenshan, eastern Tibetan plateau. Tectonophysics 619–620:143–148. doi:10.1016/j.tecto.2013.09.011

Wang G, Wei W, Ye G, Jin S, Jing J, Zhang L, Dong H, Xie C, Omisore BO, Guo Z (2017) 3-D electrical structure across the Yadong-Gulu rift revealed by magnetotelluric data: new insights on the extension of the upper crust and the geometry of the underthrusting Indian lithospheric slab in southern Tibet. Earth Planet Sci Lett 474:172–179. doi:10.1016/j.epsl.2017.06.027

Wei W, Unsworth M, Jones A, Booker J, Tan H, Nelson D, Chen L, Li S, Solon K, Bedrosian P, Jin S, Deng M, Ledo J, Kay D, Roberts B (2001) Detection of widespread fluids in the tibetan crust by magnetotelluric studies. Science 292(5517):716–719. doi:10.1126/science.1010580

Wei W, Ye G, Jin S, Deng M, Je Jing, Peng Z, Lin X, Song S, Tang B, Qu S, Chen K, Yang H, Li G (2008) Geoelectric structure of lithosphere beneath Eastern North China: features of thinned lithosphere from magnetotelluric soundings. Earth Sci Front 15(4):204–216. doi:10.1016/S1872-5791(08)60055-X

Wei W, Jin S, Ye G, Deng M, Jing J, Unsworth M, Jones AG (2010) Conductivity structure and rheological property of lithosphere in Southern Tibet inferred from super-broadband magnetotelluric sounding. Sci China Earth Sci 53(2):189–202. doi:10.1007/s11430-010-0001-7

Wei WB, Le Pape F, Jones AG, Vozar J, Dong H, Unsworth MJ, Jin S, Ye GF, Jing JN, Zhang LT, Xie CL (2014) Northward channel flow in northern Tibet revealed from 3D magnetotelluric modelling. Phys Earth Planet Inter 235:13–24. doi:10.1016/j.pepi.2014.07.004

Wu C, Yin A, Zuza AV, Zhang J, Liu W, Ding L (2016) Pre-Cenozoic geologic history of the central and northern Tibetan Plateau and the role of Wilson cycles in constructing the Tethyan orogenic system. Lithosphere 8(3):254–292. doi:10.1130/l494.1

Xiao Q, Zhao G, Dong Z (2011) Electrical resistivity structure at the northern margin of the Tibetan Plateau and tectonic implications. J Geophys Res: Solid Earth. doi:10.1029/2010JB008163

Xiao Q, Zhang J, Wang J, Zhao G, Tang J (2012) Electrical resistivity structures between the Northern Qilian Mountains and Beishan Block, NW China, and tectonic implications. Phys Earth Planet Inter 200–201:92–104. doi:10.1016/j.pepi.2012.04.008

Xiao Q, Zhang J, Zhao G, Wang J (2013) Electrical resistivity structures northeast of the Eastern Kunlun Fault in the Northeastern Tibet: tectonic implications. Tectonophysics 601:125–138. doi:10.1016/j.tecto.2013.05.003

Xiao Q, Shao G, Liu-Zeng J, Oskin ME, Zhang J, Zhao G, Wang J (2015a) Eastern termination of the Altyn Tagh Fault, western China: Constraints from a magnetotelluric survey. J Geophys Res: Solid Earth:2014. doi:10.1002/2014JB011363

Xiao W, Windley BF, Sun S, Li J, Huang B, Han C, Yuan C, Sun M, Chen H (2015b) A Tale of Amalgamation of Three Permo-Triassic Collage Systems in Central Asia: Oroclines, Sutures, and Terminal Accretion. Annual Review of Earth and Planetary Sciences 43(1):16.11–31

Xiao Q, Shao G, Yu G, Cai J, Wang J (2016) Electrical resistivity structures of the Kunlun–Qaidam–Qilian system at the northern Tibet and their tectonic implications. Phys Earth Planet Inter 255:1–17. doi:10.1016/j.pepi.2016.03.011

Xiao Q, Yu G, Liu-Zeng J, Oskin ME, Shao G (2017) Structure and geometry of the Aksay restraining double bend along the Altyn Tagh Fault, northern Tibet, imaged using magnetotelluric method. Geophys Res Lett 44(9):4090–4097. doi:10.1002/2017GL072581

Xie C, Jin S, Wei W, Ye G, Jing J, Zhang L, Dong H, Yin Y, Wang G, Xia R (2016) Crustal electrical structures and deep processes of the eastern Lhasa terrane in the south Tibetan plateau as revealed by magnetotelluric data. Tectonophysics 675:168–180. doi:10.1016/j.tecto.2016.03.017

Xiong X, Gao R, Li Y, Hou H, Liang H, Li W, Guo L, Lu Z (2015) The lithosphere structure of the Great Xing'an Range in the eastern Central Asian Orogenic Belt: constrains from the joint geophysical profiling. J Asian Earth Sci 113:481–490. doi:10.1016/j.jseaes.2015.06.006

Xu GJ, Tang J, Huang QH, Makoto U (2015) Study on the conductivity structure of the upper mantle and transition zone beneath North China. Chinese Journal of Geophysics- Chinese Edition 58(2):566–575

Xu Y, Yang B, Zhang S, Liu Y, Zhu L, Huang R, Chen C, Li Y, Luo Y (2016a) Magnetotelluric imaging of a fossil paleozoic intraoceanic subduction zone in western Junggar, NW China. J Geophys Res: Solid Earth doi:10.1002/2015JB012394

Xu Y, Zhang S, Griffin WL, Yang Y, Yang B, Luo Y, Zhu L, Afonso JC, Lei B (2016b) How did the Dabie Orogen Collapse? Insights from 3D Magnetotelluric Imaging of Profile Data. J Geophys Res: Solid Earth doi:10.1002/2015JB012717

Yin A (2010) Cenozoic tectonic evolution of Asia: a preliminary synthesis. Tectonophysics 488(1–4):293–325. doi:10.1016/j.tecto.2009.06.002

Yin Y, Jin S, Wei W, Santosh M, Dong H, Xie C (2016) Construction and destruction of the North China Craton with implications for metallogeny: magnetotelluric evidence from the Hengshan–Wutai–Fuping region within Trans-North China Orogen. Gondwana Res 40:21–42. doi:10.1016/j.gr.2016.08.001

Yin Y, Wei W, Jin S, Santosh M (2017) Fossil oceanic subduction zone beneath the western margin of the Trans-North China orogen: magnetotelluric evidence from the Lüliang Complex. Precambrian Research:Inpress doi:https://doi.org/10.1016/j.precamres.2017.01.012

Yoshimura R, Oshiman N, Uyeshima M, Ogawa Y, Mishina M, Toh H, Sakanaka Sy, Ichihara H, Shiozaki I, Ogawa T, Miura T, Koyama S, Fujita Y, Nishimura K, Takagi Y, Imai M, Honda R, Yabe S, Nagaoka S, Tada M, Mogi T (2008) Magnetotelluric observations around the focal region of the 2007 Noto Hanto Earthquake (Mj 6.9), Central Japan. Earth, Planets and Space 60(2):117–122 doi:10.1186/bf03352771

Yoshimura R, Oshiman N, Uyeshima M, Toh H, Uto T, Kanezaki H, Mochido Y, Aizawa K, Ogawa Y, Nishitani T, Sakanaka S, Mishina M, Satoh H, Goto T, Kasaya T, Yamaguchi S, Murakami H, Mogi T, Yamaya Y, Harada M, Shiozaki I, Honkura Y, Koyama S, Nakao S, Wada Y, Fujita Y (2009) Magnetotelluric transect across the Niigata-Kobe Tectonic Zone, central Japan: A clear correlation between strain accumulation and resistivity structure. Geophys Res Lett. doi:10.1029/2009GL040016

Zeng S, Hu X, Li J, Xu S, Fang H, Cai J (2015) Detection of the deep crustal structure of the Qiangtang terrane using magnetotelluric imaging. Tectonophysics 661:180–189. doi:10.1016/j.tecto.2015.08.038

Zhan Y, Zhao G, Unsworth M, Wang L, Chen X, Li T, Xiao Q, Wang J, Tang J, Cai J, Wang Y (2013) Deep structure beneath the southwestern section of the Longmenshan fault zone and seimogenetic context of the 4.20 Lushan M S7.0 earthquake. Chin Sci Bull 58(28):3467–3474. doi:10.1007/s11434-013-6013-x

Zhang L-T, Jin S, Wei W-B, Ye G-F, Duan S-X, Dong H, Zhang F, Xie C-L (2012) Electrical structure of crust and upper mantle beneath the eastern margin of the Tibetan plateau and the Sichuan basin. Chin J Geophys-Chin Ed 55(12):4126–4137

Zhang L, Jin S, Wei W, Ye G, Jing J, Dong H, Xie C (2015a) Lithospheric electrical structure of South China imaged by magnetotelluric data and its tectonic implications. J Asian Earth Sci 98:178–187. doi:10.1016/j.jseaes.2014.10.034

Zhang L, Unsworth M, Jin S, Wei W, Ye G, Jones AG, Jing J, Dong H, Xie C, Le Pape F, Vozar J (2015b) Structure of the Central Altyn Tagh Fault revealed by magnetotelluric data: new insights into the structure of the northern margin of the India-Asia collision. Earth Planet Sci Lett 415:67–79. doi:10.1016/j.epsl.2015.01.025

Zhang L, Ye G, Jin S, Wei W, Unsworth M, Jones AG, Jing J, Dong H, Xie C, Le Pape F, Vozar J (2015c) Lithospheric electrical structure across the Eastern segment of the Altyn Tagh fault on the Northern margin of the Tibetan Plateau. Acta Geologica Sinica–English Ed 89(1):90–104. doi:10.1111/1755-6724.12397

Zhang H, Huang Q, Zhao G, Guo Z, Chen YJ (2016) Three-dimensional conductivity model of crust and uppermost mantle at the northern Trans North China Orogen: evidence for a mantle source of Datong volcanoes. Earth Planet Sci Lett 453:182–192. doi:10.1016/j.epsl.2016.08.025

Zhao G, Unsworth MJ, Zhan Y, Wang L, Chen X, Jones AG, Tang J, Xiao Q, Wang J, Cai J, Li T, Wang Y, Zhang J (2012) Crustal structure and rheology of the Longmenshan and Wenchuan Mw 7.9 earthquake epicentral area from magnetotelluric data. Geology 40(12):1139–1142. doi:10.1130/g33703.1

Zheng T, Zhao L, Zhu R (2009) New evidence from seismic imaging for subduction during assembly of the North China craton. Geology 37(5):395–398. doi:10.1130/g25600a.1